https://doi.org/10.5194/egusphere-2026-2964
Preprint. Discussion started: 21 July 2026

Carbon Cycle Perturbance During the Carnian Pluvial Episode (Larne Basin, Northern Ireland)

Marwa Mohamed Shahid[1,2], Aisha Al Suwaidi[1,2], Frantz Ossa Ossa[1,2,3], Micha Ruhl[4], Amanda Perera[4], Robert Raine[5], Yongdong Wang[6] and Qing Li[7]

[1]Earth Sciences Department, Khalifa University of Science and Technology, Abu Dhabi, United Arab Emirates.
[2]Polar Research Center, Khalifa University of Science and Technology, Abu Dhabi, United Arab Emirates.
[3]Department of Geology, University of Johannesburg, 2092 Johannesburg, South Africa.
[4]Department of Geology and Research Ireland Centre for Applied Geosciences (iCRAG), School of Natural Sciences, Trinity College Dublin, The University of Dublin, College Green, Dublin 2, Ireland.
[5]British Geological Survey, Belfast, Northern Ireland.
[6]Nanjing Institute of Geology and Palaeontology, Chinese Academy of Sciences, Nanjing, China.
[7]The 11th Geological Brigade of Sichuan, Chengdu, China.

Correspondence to: Marwa M. Shahid (marwashahid123@gmail.com)

Abstract. The Late Triassic Carnian Pluvial Episode (CPE, ~232 Ma) marks a major global climatic transition characterized by intensification of humid conditions following a prolonged period of aridity through much of the Triassic. This episode triggered profound environmental and biotic change that ushered in modern environments and ecosystems. Here, we present a new integrated high-resolution geochemical and sedimentological record from the Knocksoghey Formation, Mercia Mudstone Group, in the Larne Basin, Northern Ireland. The high-resolution organic carbon isotopes document a ~4‰ negative excursion, whose onset coincides with a small, reproducible rise in Hg concentrations from background levels, thought to be associated with the emplacement of the Wrangellia Large Igneous Province (LIP). The geochemical anomalies stratigraphically closely precede a pulse of coarse siliciclastics, indicative of intensified weathering driven by enhanced rainfall, and are followed by a return to arid, restricted conditions, marked by deposition of stacked anhydrite nodules and beds. The CPE was previously suggested to be characterized by a succession of negative carbon isotope excursions (NCIEs) in sedimentary archives. However, our new data demonstrates a more protracted stepped carbon cycle perturbance, as reflected by a single, stratigraphically prolonged carbon isotope excursion, comparable in nature to NCIEs observed during other LIP-driven climatic perturbations, such as the Toarcian Oceanic Anoxic Event.

1 Introduction

The Late Triassic Carnian Pluvial Episode (CPE, ~232 Ma) has been described as a prolonged episode of drastic climatic transition from arid to more wet and humid conditions. This climatic transition occurred synchronously with a period of major reorganization of the Earth's biota, both on land and in marine environments, resulting in the widespread extinction of some species and dominance of others (Ruffell et al., 2016; Bernardi et al., 2018; Dal Corso et al., 2020). Among the most striking changes was the diversification and increase in dinosaur population, whereby they replaced the previously dominant

https://doi.org/10.5194/egusphere-2026-2964
Preprint. Discussion started: 21 July 2026

herbivores (Nesbitt et al., 2017; Bernardi et al., 2018; Benton et al., 2018). This interval also marks the renewed appearance of coal after the prolonged global 'coal gap' that followed the Permo–Triassic terrestrial ecosystem collapse, indicating the reestablishment of environments conducive to peat accumulation (Retallack et al., 1996; Dal Corso et al., 2020; Zhang et al., 2023). The first appearance of amber in the fossil record is also noted in the Carnian, with greater amber preservation typically occurring in the presence of environmental stressors and under wet conditions (cf. Fischer et al., 2017; Seyfullah et al., 2018). With the coinciding transition to coral-dominated reef systems (Dal Corso et al., 2015) and the rise of modern mammals (Datta, 2005; Lecuona et al., 2016) and calcispheres (Preto et al., 2014), the CPE is proposed to represent the peak of recovery following the end-Permian mass extinction (~252 Ma), and to have laid the foundation for modern ecosystems (Callegaro et al., 2023).

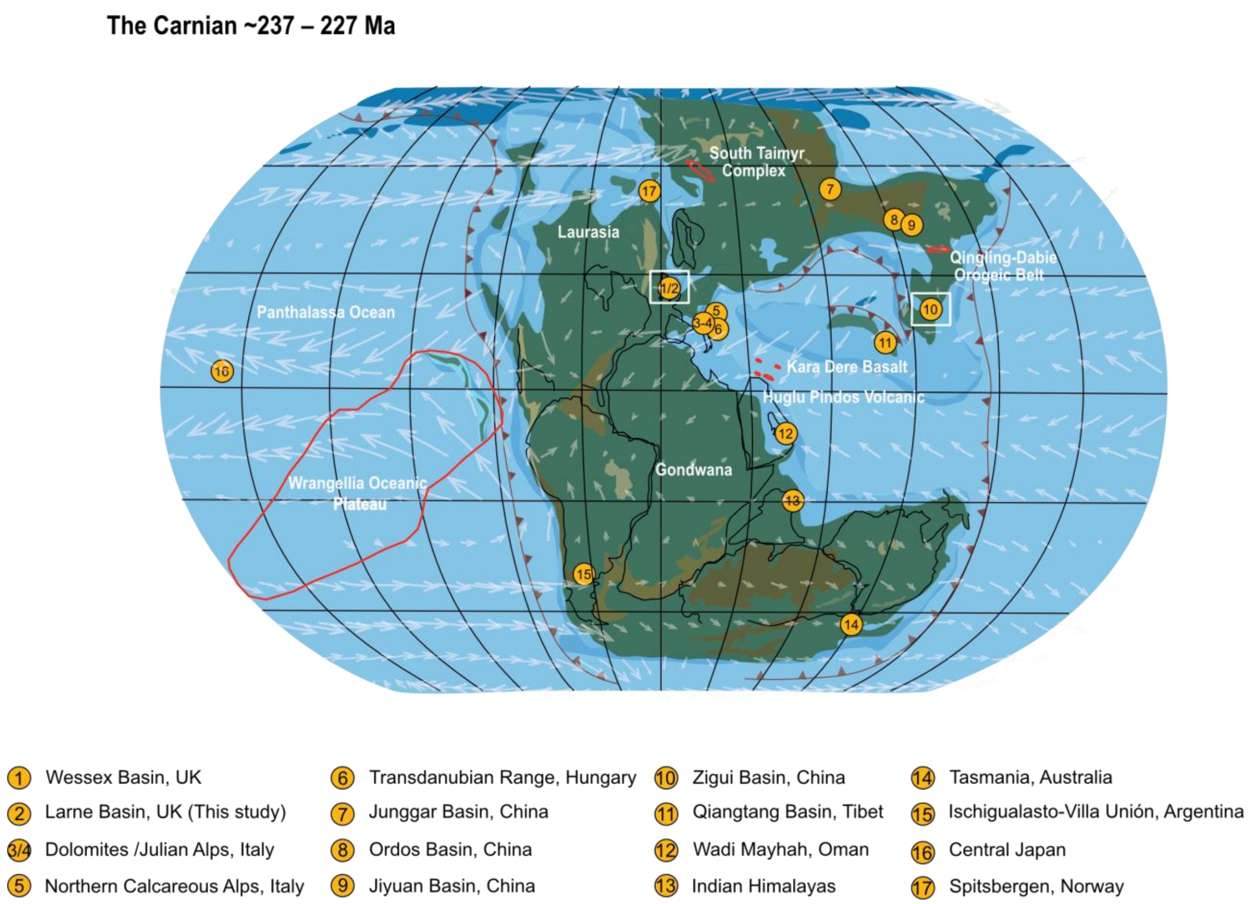

Figure 1: Reconstructed Carnian paleogeographic map showing the locations of active Large Igneous Provinces (LIPs) (red outline) and subduction zones (brown arrows and lines). White arrows indicate modeled near-surface wind patterns prior to the Carnian Pluvial Episode (CPE), modified from Zhao et al. (2025). Yellow numbered symbols mark sedimentary successions and basins that record a negative $\delta^{13}C$ excursion linked to the CPE. White boxes denote the locations discussed in the present study.

https://doi.org/10.5194/egusphere-2026-2964
Preprint. Discussion started: 21 July 2026

Marked records from (1) Miller et al., 2017 (2) This study (3–6) Dal Corso et al., 2018 (7) Zhao et al., 2025 (8) Rahman et al., 2024 (9) Lu et al., 2021 (10) Li et al., 2022 (11) Zhang et al., 2024b (12) Sun et al., 2019 (13) Hornung et al., 2007 (14) Lestari et al., 2024 (15) Mancuso et al., 2020; Pedernera et al., 2026 (16) Tomimatsu et al., 2021 (17) Mueller et al., 2016.

The CPE is dated to ca. 234–232 Ma based on biostratigraphy, cyclostratigraphy, magnetostratigraphy, and zircon U-Pb dating, with an estimated duration of 0.8–1.6 Myr (e.g., Zhang et al., 2015; Miller et al., 2017; Zhang et al., 2024b; Zhao et al., 2025). The onset of the CPE is marked by various proxies in marine and continental strata, such as the occurrence of the initial carbon isotope excursion of ~2–7‰ at the Julian 1/Julian 2 boundary, corresponding to the appearance of *Austrotrachyceras austriacum* ammonoids, an influx of coarse siliciclastics, and a widespread shift to hygrophytic palynological assemblages from xerophytic ones (Roghi et al., 2010; Mueller et al., 2016; Bernardi et al., 2018; Dal Corso et al., 2018, 2020; Mazaheri-Johari et al., 2021; Baranyi et al., 2025). The carbon cycle perturbations associated with the CPE, commonly labeled NCIE 1–4, have been proposed to span the interval from the late Julian 1 to the mid-Tuvalian, with NCIE-4 placed at the base of, or within, Tuvalian 2 (Dal Corso et al., 2020). The NCIEs associated with the CPE are thought to have been driven by perturbance of the global carbon cycle, associated with the emplacement of the Wrangellia Large Igneous Province (W-LIP) in the North Pacific and amplified by subsequent Earth system feedbacks (Dal Corso et al., 2020; Lu et al., 2021; Mazaheri-Johari et al., 2021). Despite the significance of this climatic event, detailed geochemical studies linking the CPE to Wrangellia remain scarce, largely due to limited chronostratigraphic control for Wrangellia and the global sedimentary records of the episode.

Here, we present new high-resolution geochemical data, including stable organic carbon isotope measurements, Hg/TOC ratios, and XRF-derived elemental concentrations integrated with detailed sedimentological descriptions from the Knocksoghey Formation of the Triassic Mercia Mudstone Group of Northern Ireland, studied in the Carnduff-1 (CRN-1) core of the Larne Basin.

2 Geological setting and litho- and chronostratigraphy

Upper Triassic stratigraphy in Northern Ireland is found across the Rathlin, Lough Foyle, Larne, and Lough Neagh basins. Larne and Lough Neagh are interconnected basins, with an interbasinal high separating their main depocentres (Raine et al., 2021; Fig. 2. A (map inset)). The Larne Basin, situated within the Midland Valley terrane, extending between Northern Ireland and southwest Scotland, is a NE-SW trending half-graben that is likely to have formed during the early extension phase of the breakup of Pangea (Jeram et al., 2021). While part of the basin lies onshore in Northern Ireland, it also continues offshore into the North Channel seaway (Shelton, 1997). The Mercia Mudstone Group (MMG) is dominated by red to brown mudstone, with some green and grey mudstone and siltstone. The MMG is sandwiched between the lower Triassic fluvial/lacustrine Sherwood Sandstone Group and the uppermost Triassic marine Westbury Formation of the Penarth Group (Mitchell, 2004; English et al., 2024). The MMG in Northern Ireland has been divided into six formations, namely Lagavarra, Craiganee, Glenstaghey, Knocksoghey, Port More, and Collin Glen Formations (Wilson and Manning, 1978; Penn et al., 1983). This study is primarily concerned with the uppermost Glenstaghey and Knocksoghey Formations of the

MMG sampled from the Carnduff-1 (CRN-1) borehole. Sandstone units of up to 2.5 m thickness, locally referred to as "skerries," occur higher in the MMG, and the Knocksoghey Formation houses the Coolmaghra Skerry Member (Simms, 2009).

CRN-1 was drilled in 2013 within the Larne Basin, in the eastern part of County Antrim (54.837°N, 5.819°W). The core passes through almost the entire Mercia Mudstone Group to the base of the Glenstaghey Formation (Boomer et al., 2021). Previous studies of the nearby Carnduff-2 borehole (CRN-2; 54.839°N, 5.821°W) have provided insights into the depositional setting of the Mercia Mudstone Group (Andeskie et al., 2018). $\delta^{34}S_{evap}$ data from the Glenstaghey and lower Knocksoghey Formations indicate extended intervals during deposition when evaporitic brines were hydrologically isolated from the global seawater sulfate reservoir, consistent with a dominantly continental/terrestrial depositional setting (Salisbury et al., 2025). Additional studies on the Carnduff boreholes have established a detailed litho- and chronostratigraphic framework (Raine et al., 2021), with carbon and oxygen stable isotope records integrated with ammonite, calcareous microfossil, and ostracod analyses providing a high-resolution, multi-proxy biostratigraphic framework for the uppermost Triassic and lower Jurassic marine successions in the Larne Basin (Boomer et al., 2021).

The sedimentological work of Andeskie et al. (2018) indicates that continental deposition occurred in saline lakes, saline mudflats, dry mudflats, and desert paleosols, where processes such as flooding, evaporation, and wind played dominant roles. They concluded that the depositional environments were extreme, based on the sparsity of roots, bioturbation, and fossils, as well as the prevalence of evaporites like halite, anhydrite, and gypsum within the MMG. The higher sandstone content in the upper interval of the MMG has been suggested to indicate a transitional trend from a lake-dominated to an aeolian-dominated depositional system (Andeskie et al., 2018). An aeolian origin is also suggested as its bedding characteristics and particle size trends closely resemble wind-deposited red clay from the Chinese Loess Plateau (Mao et al., 2021), or the modern endorheic depositional setting of the Kati Thanda-Lake Eyre system of Australia (English et al., 2024). The continental depositional environment terminated during late Rhaetian times, with the flooding of the continental rift basins of Britain and Ireland in response to (eustatic) sea level rise, which established the marine deposition of the latest Triassic Westbury and Lilstock Formations of the Penarth Group and the Early Jurassic Waterloo Mudstone Formation of the Lias Group (Warrington and Ivimey-Cook, 1992).

Although macrofossils are largely absent from the Mercia Mudstone succession in Northern Ireland due to the oxidizing red-bed depositional environment, palynomorphs recovered from a few horizons provide some age control (Merlin Energy Resources Consortium, 2020). Deposition of the MMG occurred from the Middle Triassic Anisian to Late Triassic Carnian to intra-Rhaetian (Howard et al., 2008), with the overlying Penarth Group assigned to the Late Rhaetian (Warrington, 1995). The Knocksoghey and upper Glenstaghey Formations of the MMG are considered laterally equivalent to the Sidmouth Mudstone, Dunscombe Mudstone, and lower Branscombe Mudstone of Southern England, which are considered Ladinian to Carnian based on limited palynology and magnetostratigraphy (Hounslow and Gallois, 2023). The units here studied in the CRN-1 borehole include the uppermost Glenstaghey Formation and the Knocksoghey Formation. These formations have been shown to contain miospores of Ladinian to Carnian age in the neighboring Larne-2 borehole (Warrington, 1995; Mitchell, 2004).

3 Methods

Core description and sampling of the CRN-1 core were carried out at the British Geological Survey of Northern Ireland in Belfast. The core, which was unslabbed, was broken with a rock hammer and chisel. A total of 442 samples, spanning depths from 335.2 m to 532.2 m and covering the interval from the base of the Westbury Formation to the top of the Glenstaghey Formation, were collected for this study. Sampling was conducted at 1 m intervals between 335 m and 450 m, with the resolution increased to 0.3 m from 450 m to 532.2 m.

3.1 Major element analysis

XRF analysis was carried out on 95 pressed powder pellets using a wavelength-dispersive (WD) XRF Spectrometer (Rigaku ZSX Primus IV) equipped with an Rh (Rhodium) X-ray tube. Dried, powdered samples were mixed with Licowax binder in a 9:1 (sample to binder) ratio and pressed into 40 mm aluminium cups. A pressure of 10–12 tonnes was applied for ~60 s to pelletize the samples. NIST 2711a was used as the reference standard, with the standard rerun after every 10 samples. Additionally, one sample was reanalyzed together with NIST 2711a for quality control. Replicate analysis yielded standard deviations of 0.48% for Al_2O_3, 0.5% for CaO, 0.33% for Fe_2O_3, 0.19% for K_2O, 0.5% for MgO, 0.007% for MnO, 1.7% for SiO_2, 1.52% for Na_2O, 0.02% for P_2O_5, and 0.1% for TiO_2.

3.2 Organic carbon isotope and Total Organic Carbon (TOC)

Prior to isotope analysis, samples were manually crushed using an agate mortar and pestle, refluxed at 60°C with 3M HCl for 4 hours, and then left to decarbonate overnight with a fresh aliquot of 3M HCl. The following day, the acid was decanted, and the samples were rinsed with 40 mL aliquots of deionized water until neutralized. The neutralized residues were left to dry in an oven at 50°C, and once dry, re-crushed to break up lumps, transferred to microtubes, and sealed until analysis.

$\delta^{13}C_{TOC}$ and TOC content for 256 samples from 376–532.2 m were analyzed at the Department of Geology, Trinity College Dublin, The University of Dublin. Due to the low TOC content of the samples, about 50 mg of the decarbonated fraction was weighed and prepared for analysis. L-Alanine ($\delta^{13}C_{org}$ = -25.119‰) was used as the reference standard for the calibration of values, and EMA-P2 (ethylene methacrylate) ($\delta^{13}C_{org}$ = -28.19‰) was employed as the quality standard, which is reported in per mil (‰), relative to Vienna Pee Dee Belemnite (VPDB). Replicate analysis of EMA-P2 yielded a standard deviation (1σ) of ±0.33‰ for δ13CTOC and ±1.12 % for TOC.

3.3 Mercury Analysis

Mercury concentrations were determined for 375 samples (370.65–532.2 m) from the Carnduff-1 core using a LECO AMA-254 Advanced Mercury Analyzer at the Earth Surface Research Laboratory (ESRL) at the Department of Geology, Trinity

College Dublin, The University of Dublin. Analysis was carried out at ~1 m sample spacing in the first half of the core, extending to 450 m, after which the resolution was increased to ~30 cm. Approximately 150-200 mg of the sample was weighed into tin boats. Because low Hg concentrations were suspected, all samples were measured in 'blank-mode', and mercury concentration values (in ppb) were subsequently calculated offline. NIST 1515 (Apple Leaves; Hg = 43.2 ± 2.3 ppb) was used as the reference standard. ERM-CD 281 (Ryegrass; Hg = 16.4 ± 2.2 ppb) was analyzed at the start, middle, and end of each run for quality control, yielding a standard deviation of ± 0.6 ppb (2σ).

For the Hubei dataset, a set of 63 powdered rock samples, with ~30 cm spacing in the lower 34 m of the section and ~2 m spacing in the remaining part of the section, was analyzed in the same laboratory. An average of ~104 mg per sample was weighed on a scale. Nine samples were measured in duplicate. The average standard deviation of the duplicate measurements is 0.2 ppb, and the difference value between two duplicates of a sample is ~2.16%. Reference standard ERM-CD281 (with a certified value of 16.4 ppb) was analyzed 25 times, with an average measured value of 17.7 ppb and a standard deviation of 0.76 ppb. An internal standard was measured six times. The standard deviation on the internal standard is 0.38 ppb, for an average value of 146.3 ppb.

4 Results

4.1 Lithostratigraphy and geochemistry of the CRN-1 borehole

In the CRN-1 borehole, the Knocksoghey Formation consists of massive, reddish-brown mudstones, with rare to absent sedimentary structures. Throughout the unit, these mudstones contain distinctive green reduction spots, which are common at the base of the unit, where highly reduced fine sandy-silty mudstone dominates, with a decreasing occurrence upward in stratigraphy. Anhydrite nodules and beds, displacive halites, and gypsum are common throughout the succession, with an increase in the upper part of the Knocksoghey Formation (455–390 m), interpreted to indicate an overall evaporitic depositional environment (Andeskie et al., 2018).

A notable lithological change occurs between 477–466 m in the Knocksoghey Formation, where the otherwise monotonous, reddish-brown, very fine mudstone deposits are overlain by fine- to medium-grained sandstone and grey-green siltstone units interbedded with bioturbated grey sandy-mud, together forming a ~10 m thick interval known as the Coolmaghra Skerry Member (Fig. 2). The first prominent increase in Si content occurs at a depth of ~485 m, followed by a second increase at ~482 m. Discrete sandstone beds are present at ~477, 476, and 475 m, each ~50 cm thick, together forming an ~2 m-thick interbedded sandstone package, comparable to the ~1.7 m sandstone interval reported from the neighboring CRN-2 borehole (Andeskie et al., 2018). The very fine to coarse-grained sandstones are angular to well-rounded and exhibit moderate to poor sorting. The sand is locally clean but shows evidence of bioturbation and minor pedogenic alteration, becoming noticeably coarser towards the top of the interval. The uppermost sandy bed, positioned at ~466 mbs in CRN-1, is poorly cemented and interbedded with a mudstone interval ~10 cm in thickness. Following this, the lithological composition returns to the

https://doi.org/10.5194/egusphere-2026-2964
Preprint. Discussion started: 21 July 2026

monotonous reddish-brown mudstone, with within-bed anhydrite crystals reappearing at ~456.5 mbs, approximately 8.5 m above the final sandy interval, with the anhydrite occurrence increasing upwards through the Knocksoghey Formation.

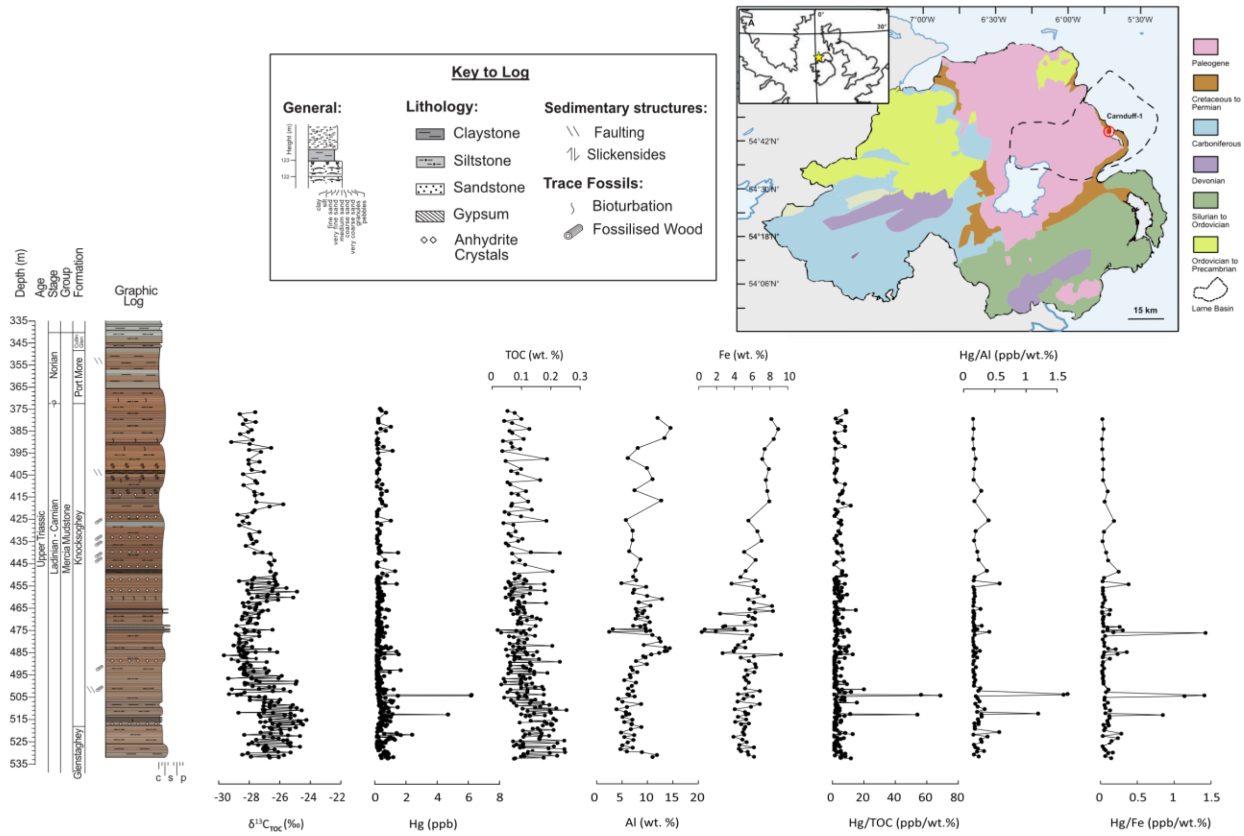

Figure 2: Lithostratigraphy and geochemical profiles for the Knocksoghey Formation in the Carnduff-1 core. From left to right: Graphic log (depth, m); the superimposed color variations through the core were obtained by scanning powdered samples. Bulk organic carbon isotopes ($\delta^{13}C_{TOC}$; ‰ VPDB), Hg (ppb), total organic carbon (TOC, wt.%), Al (wt.%), Fe (wt.%), Hg/TOC (ppb per wt.%), Hg/Al (ppb per wt.%), and Hg/Fe (ppb per wt.%). The interval interpreted as the Carnian Pluvial Episode (CPE) shows a stepwise negative $\delta^{13}C_{org}$ excursion accompanied by discrete Hg and Hg/TOC enrichments, followed by a lithological shift to coarser siliciclastics.

Top right corner: Geological map of Northern Ireland showing bedrock distribution (adapted from Cooper et al., 2018, BGS Report CR/17/096). The dashed black lines outline the approximate extent of the Larne Basin. The red circular target shows the location of the Carnduff-1 borehole. Inset A: Paleolocation of Northern Ireland during the CPE, with the paleolatitude indicated (Modified after Scotese, 2013).

X-ray fluorescence (XRF) analysis was conducted on 95 sample pellets to determine their elemental composition and analyze the weathering scenario and climatic conditions during sedimentary deposition. Across the studied interval, major

https://doi.org/10.5194/egusphere-2026-2964
Preprint. Discussion started: 21 July 2026

oxides show wide compositional variability. With depth, there is a systematic variance of these oxides, reflecting alternation between terrigenous sandstone beds and Na-Ca-Mg-rich playa/evaporitic facies. In the studied section, except for a few samples near the Coolmaghra Skerry Member, nearly all samples exhibit very high Na concentrations (~15–20 wt.%). The absence of any systematic decrease in Na_2O up section suggests that Na mobility is primarily controlled by brine chemistry and evaporite precipitation, rather than by silicate weathering. Measured Cl contents covary with Na, indicating that halite salts are the most likely source of elevated Na, consistent with the occurrence of displacive halite throughout the Knocksoghey Formation in the neighboring Carnduff-2 core (Andeskie et al., 2018).

Geochemical weathering indices are used to characterize stratigraphic variances in weathering indicators by incorporating oxides of major elements, thereby providing a visual representation of changes in sediment composition (Price and Velbel, 2003). All of the indices show a consistent and pronounced excursion in the interval from ~475–485 m, where the sandstone beds interrupt the otherwise dominantly mud-rich stratigraphic succession (Fig. 3). In this interval, CIA, CIW, CPA, PIA, and V reach their maxima, while WIP and Index B attain their minimum values. CIA values increase from ~13 in the lower part of the succession to 50–60 between 475–485 m, while PIA increases from ~5–10 to values up to 74. However, CIW and CPA exhibit higher values for the same stratigraphic interval in the core. CIW increases from 10–15 in the lower part of the core, to values up to 85 in this interval, before decreasing again to ~10 above ~475 m. Similarly, CPA values also increase from 15–20 from the lower Knocksoghey Formation, to ~82 between 475–485 m, followed by a return to pre-excursion values. Vogt's index also rises from 0.1 to 0.8–1, while WIP (~20) and Index B values (0.3–0.4) remain low across the interval.

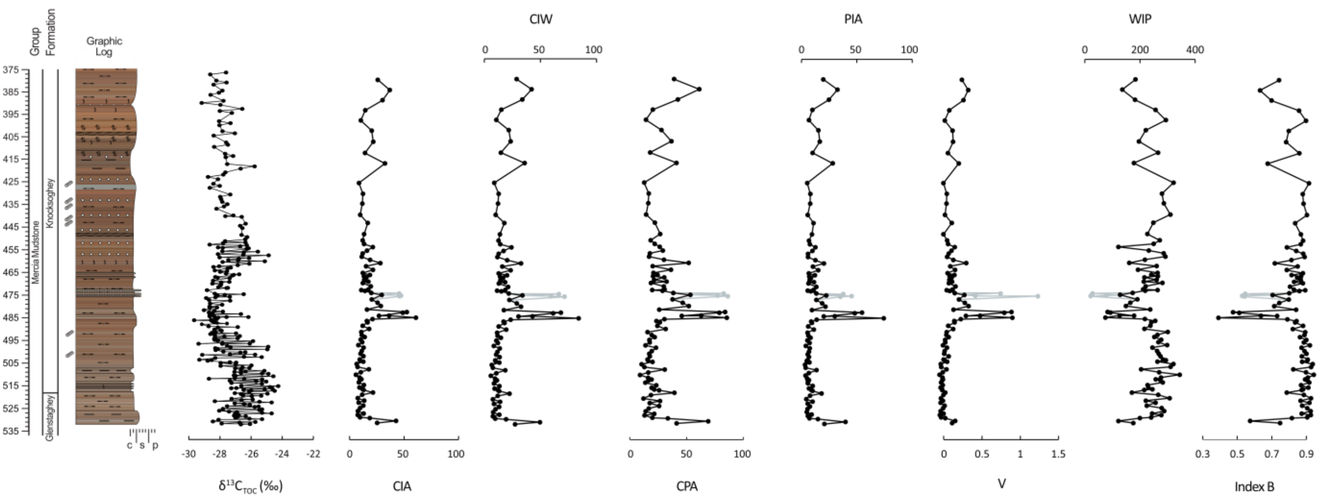

Figure 3: Variation of geochemical weathering indices for the uppermost Glenstaghey and the Knocksoghey Formations. The calculated indices are CIA (Chemical Index of Alteration), CIW (Chemical Index of Weathering), CPA (Chemical Proxy of Alteration), PIA (Plagioclase Index of Alteration), V (Vogt's Index), WIP (Weathering Index of Parker), and Index B. The grey data points represent sandstone samples.

TOC values are relatively low throughout the studied section, with values ranging from 0.02 wt.% (474.42 m) to 0.25 wt.% (529.3 m), averaging at around 0.11 wt.% (Fig. 2). A total of 256 samples, comprising the uppermost Glenstaghey Formation and almost the entire Knocksoghey Formation, from 376.02–532.2 m in the CRN-1 core, were analyzed for their $\delta^{13}C_{TOC}$ composition. Obtained $\delta^{13}C_{TOC}$ values range from -24.1‰ to -29.5‰, with an average value of -27.1‰. The $\delta^{13}C_{TOC}$ shows a ~3‰ positive trend from 532.2–509.75 m, which is interrupted by a negative excursion with values as low as -29.5‰. The onset of the negative excursion begins at around 508.4 m, prior to the interruptive sandstone beds, and ends at around 449 m, with up to ~4‰ change relative to pre-excursion values, followed by a recovery period.

Bulk mercury concentrations are significantly low across the studied interval, ranging from 0.07 ppb (at ~496.3 m) to 6.2 ppb (at 503.62 m), with a mean value of 0.3 ppb (Fig. 2). The background Hg concentration for the sample set is 0.224 ppb, calculated using the iterative 2σ technique discussed in Matschullat et al. (2000). Both Hg and Hg/TOC show a small peak, with values of 4.7 ppb and 47 ppb/wt.% at 512.45 m immediately prior to the negative excursion, followed by a second spike with values up to 6.2 ppb and 68.6 ppb/wt.%, respectively, coinciding with the onset of the NCIE. The Hg/TOC record overall mirrors the trends in Hg concentration.

We also present a new CPE Hg record from the Luojiagou section in Hubei, China. Overall, Hg concentrations are low (Fig. 5), ranging from 0.4–89.4 ppb, with an average of 11.15 ppb. Similarly, Hg/TOC ratios display a low background, ranging from 3.95 to 1327.4 ppb/wt.% with a mean of ~170 ppb/wt.%. Slightly after the onset of the NCIE, Hg values increase from <5 ppb to peaks of ~30-58 ppb, while Hg/TOC rises from ~30–40 ppb/wt.% to ~100 ppb/wt.%, at the onset of the excursion and locally reaches 1327.4 ppb/wt.%. High Hg/TOC levels (>500 ppb/wt.%) persist throughout the NCIE before declining upsection.

5 Discussion

5.1 Lithostratigraphic evolution of the Carnian stratigraphy in the Larne Basin (Northern Ireland)

The Carnian Pluvial Episode was initially identified based on the presence of fluvial sandstone units in the North Curry Sandstone Member within the Mercia Mudstone Group, which interrupted the otherwise arid and semi-arid playa-lake sediments that characterized the Upper Triassic of the UK (Simms and Ruffell, 2018). Similar facies were observed in late Carnian units across the British Triassic, which correlated with the 35 m thick Schilfsandstein unit of the German Keuper succession that overlaid playa-lake mudstones (Simms and Ruffell, 1989; 1990), which was later recorded in multiple sedimentary successions globally (e.g., Boulvain et al., 2001; Arche and López-Gómez, 2014; Simms and Ruffell, 2018; Jin et al., 2019). The interbedded sand and mud units within the lower Knocksoghey Formation of the MMG and equivalent units in sedimentary basins across Northern Ireland, England, and Wales (Sidmouth, Branscombe, Dunscombe Fm.) have long been considered to represent the CPE (cf. Simms and Ruffell, 1989; Simms and Ruffell, 2018; Baranyi et al., 2019; Ruffell and Kürschner, 2020). The ~10 m thick bed of interbedded sandstone and mudstone layers of the Coolmaghra Skerry Member has therefore indeed been suggested to be equivalent to the Arden Sandstone and the Schilfsandstein units (Simms,

https://doi.org/10.5194/egusphere-2026-2964
Preprint. Discussion started: 21 July 2026

2009). The sandstone beds within the Knocksoghey Formation in the Carnduff-1 core are indicative of a shift in the prevailing climate and can be interpreted as pulses of enhanced terrigenous flux delivered during the CPE. Terrigenous proxies such as Si/Al, Zr/Al, and (Rb+Zr)/Sr (e.g., Ratcliffe et al., 2012; Yang et al., 2016; Mansour et al., 2022) all reach local maxima within this interval (Fig. A1), coincident with peak values in the major-element weathering indices.

Geochemical weathering indices are dimensionless numbers that depend on the depletion of more mobile elements and the enrichment of less mobile ones during weathering. Due to their formulation, different weathering indices respond differently to progressive chemical alteration. Indices such as CIA (Chemical Index of Alteration), CIW (Chemical Index of Weathering), CPA (Chemical Proxy of Alteration), PIA (Plagioclase Index of alteration), and Vogt's index (V) increase as labile cations (Ca, Na, K, Mg) are removed relative to the more immobile Al-bearing framework, whereas indices such as WIP (Weathering Index of Parker), ICV (Index of Compositional Variability), and Index B decrease as weathering proceeds. Depth profiles of these indices for the Knocksoghey Formation (Fig. 3) provide an integrated view of both the intensity and vertical distribution of chemical weathering in the core. A key complication in this case is that the commonly employed geochemical indices use Na_2O (and CaO) concentrations in their formulas, assuming that these oxides primarily reside in silicate minerals. In this sample set, however, Na and Ca are also hosted in abundant non-silicate phases, including halite, gypsum, anhydrite, and other salts and carbonates. These added salts and carbonates artificially lower the values of these indices, making the rocks appear to be 'poorly weathered' when, in reality, their chemistry is heavily modified by the addition of base cations from brines. This effect is expressed by the extremely low index values observed through most of the core. Even basement rocks or weakly to moderately pre-weathered source rocks would be expected to yield CIA and CPA values of ~50 (e.g., Tosca et al., 2010). Therefore, the much lower values recorded for the samples in this study are unlikely to reflect primary source rock weathering intensity. Between ~475 and 485 m, however, Na_2O content drops sharply (up to 0.6 wt.%) to commonly observed values, with little to no contribution from evaporitic phases. Measured Na values in samples from this interval are therefore assumed to indicate Na hosted primarily in the silicate fraction, outside of which none of the Na-based weathering indices can be employed as a straightforward measure of progressive silicate weathering.

Although the samples in this interval show the highest CIA and PIA values across the studied section of the core, their absolute values indicate only moderate degrees of weathering. Almost all calculated CIA values are ≤ 50, and only a single sample shows a CIA value of ~68, which is still below the 70–100 range typical of moderately to deeply weathered profiles. The same applies to the calculated PIA values, along with Vogt's (V) index, which also lie predominantly within the 'fresh to weakly weathered' range. In contrast, CIW and CPA yield substantially higher values, exceeding 80 and approaching the theoretical maximum of 100. These indices have the added advantage of excluding K from the weathering equation, thereby reducing issues with K mobility and related processes such as illitization and metasomatism (Price and Velbel, 2003; Buggle et al., 2011). In addition, CPA avoids the uncertainties related to CaO* corrections by excluding Ca from its formula. The lower CIA and PIA values within the same interval are therefore likely associated with post-depositional addition of K. Corresponding low Index-B values in the same interval further suggest a relatively higher weathering intensity. Among the samples that indicate stronger weathering, the sandstone units must be treated with caution. Since they are prone to post-depositional alterations, they are less reliable for assessing primary geochemical signatures (Bjørlykke, 2014; Yuan et al., 2015). Nevertheless, the occurrence of abrupt, clean, coarse-grained sandstone beds within an otherwise predominantly arid to semi-arid succession in itself provides evidence of increased silicate weathering and runoff. Further, the elevated CIW and CPA recorded in the underlying interbedded siltstone samples also indicate intensified weathering. Hence, the concordant behavior of stratigraphic trends in the CIW, CPA, and Index B proxies, with high CIW/CPA and low Index B, provides the most reliable assessment of weathering intensity across the studied interval in the Knocksoghey Formation. The observed pattern of the employed proxies indicates that, within the studied section of the succession, the samples within and in the vicinity of the Coolmaghra Skerry Member represent the interval of the strongest weathering, whereas the playa/evaporitic mudstones are strongly overprinted by the addition of cations.

The $\delta^{13}C_{TOC}$ profile across the studied interval in the CRN-1 core also attains its most negative values coincident with this interval. This negative shift and subsequent $\delta^{13}C_{TOC}$ evolution point to a perturbation of the global carbon cycle during the early Carnian, as commonly observed in sedimentary archives to occur concomitant with the CPE. Collectively, these proxies support the interpretation that the sandstone beds record a wetter, more pluvial phase and the resultant enhanced delivery of terrigenous material to the basin during the CPE. An abundance of halites and anhydrite beds and crystals above this interval indicates a return to more arid depositional conditions after the pluvial phase. This shift is mirrored in the XRF data, as Na_2O and Cl concentrations increase markedly up-section, while terrigenous proxies (Si/Al, Zr/Al, and (Rb+Zr)/Sr) decline to lower values, and weathering indices decrease, reflecting the growing dominance of precipitated salts over detrital aluminosilicates.

A similar sedimentological shift is also observed in the Dunscombe Mudstone Formation, in the geographically nearby Wiscombe Park-1 (WP-1) borehole of the Wessex Basin, SW England, which represents a shallow fluvial depositional environment (Gallois, 2008). In the WP-1 borehole, thin sandstone beds occur in three intervals at depths of approximately 58.5 m, 59.5 m, and between 61.8 m and 62.5 m (Gallois and Porter, 2006), a pattern similar to that observed in CRN-1. These sandstone beds are interpreted to be representative of the Lincombe Member, which comprises ~40–43 m of laminated mudstones, limestones, and breccias, as well as a lenticular calcareous sandstone to siltstone unit in the lower Dunscombe Mudstone Formation at the coastal type section (Gallois, 2008). The upper section of the WP-1 borehole has been assigned a Carnian (Julian 2) age (Miller et al., 2017). Although lacking a good palynological assemblage, the presence of *Triadispora verrucata* indicates an early Julian (Julian 1 age) for the lower part of WP-1. This lithological change recorded in WP-1 is also preceded by an NCIE of 3–4‰ (Miller et al., 2017).

5.2 $\delta^{13}C_{TOC}$ evolution of the Carnian in the CRN-1 borehole of the Larne Basin (Northern Ireland)

Carbon isotope records of the CPE from shallow and deeper marine, as well as terrestrial sedimentary archives globally, including China (e.g., Sun et al., 2016; Lu et al., 2021; Li et al., 2022; Zhang et al., 2024b; Zhao et al., 2025), Italy, Hungary (Dal Corso et al., 2018), UK (Miller et al., 2017), Norway (Mueller et al., 2016), Japan (Tomimatsu et al., 2021), Oman (Sun et al., 2019), Argentina (Mancuso et al., 2020; Pedernera et al., 2026) and Tasmania (Lestari et al., 2024), are commonly

https://doi.org/10.5194/egusphere-2026-2964
Preprint. Discussion started: 21 July 2026

characterized by a 2–7‰ negative shift in $\delta^{13}C$. Previous studies of the CPE have suggested that the negative shift (and negative CIE) is multi-phased, consisting of 2–5 discrete carbon isotopic events. The record from the Knocksoghey Formation of Northern Ireland studied here, in contrast, exhibits a single, prolonged, stepped negative excursion, implying a sustained ^{12}C-enriched carbon input into the biosphere, punctuated by minor variations, rather than multiple, discrete, short pulses. The ~4‰ magnitude of the observed negative shift is similar to that documented in other sections, including the neighboring Wiscombe Park-1 borehole in the UK (Miller et al., 2017). The lack of correlation between TOC and $\delta^{13}C_{TOC}$ values ($R^2 = 0.034$) suggests that neither diagenetic (thermal) alteration of the sedimentary organic matter nor organic matter source mixing played any significant role in forcing the $\delta^{13}C_{TOC}$ evolution in the studied interval of the CRN-1 core. The NCIE interrupts a longer-term ~3‰ positive excursion across the Middle–Upper Triassic in this core, which correlates to the Ladinian to Early Carnian positive trend associated with increased carbon burial and the re-establishment of coal deposition after the Early Triassic coal gap (Korte et al., 2005; Dal Corso et al., 2012).

5.3 Global C-cycle evolution during the Carnian Pluvial Episode

Although global CPE carbon isotope records are comprised of multiple negative excursions, the here obtained expanded sedimentary archive across this time interval suggests that these are not discrete and isolated events, but rather represent a prolonged stepped negative CIE interrupting an overarching positive excursion similar to what is observed for other LIP-driven events such as the Early Jurassic Toarcian CIE (T-CIE). To test this hypothesis, we compare well-constrained terrestrial and marine $\delta^{13}C_{org}$ and Hg/TOC records from the UK (Miller et al., 2017), the NW Tethys (Dal Corso et al., 2018; Mazaheri-Johari et al., 2021), Hubei – South China (*this study* and Li et al., 2022), the Jiyuan Basin – North China (Lu et al., 2021), and the Junggar Basin – NW China (Zhao et al., 2025), with the here obtained record from the CRN-1 borehole (Fig. 5 and Fig. A2). We also compare the records against the Toarcian CIE, which shares notable commonalities in magnitude and duration of the respective CIE, with observations for the Carnian Pluvial Episode.

The Toarcian negative CIE, associated with the Toarcian Oceanic Anoxic Event (T-OAE, at ~183 Ma) has also been recorded in marine, terrestrial, shallow and deep water settings worldwide, in multiple carbon reservoirs including bulk and organic carbonates, marine and terrestrial organic matter and organic compounds, with varying magnitudes of 3 to 7‰, indicating a substantial release of lighter carbon into the ocean-atmospheric system (cf. Cohen et al., 2004; Hesselbo et al., 2007; Al Suwaidi et al., 2010; Kafousia et al., 2014; Xu et al., 2018; Ruebsam et al., 2020). Similar to the CPE, the initial positive shift recorded during the T-OAE has been linked to globally increased (organic) carbon burial. The superimposed NCIE is linked to the Karoo-Ferrar Large Igneous Province (LIP), an extensive volcanic province with preserved complexes in Tasmania, Africa, and Antarctica, as well as the initiation of positive feedback processes that further affected the global exogenic carbon cycle. Studies suggest that the associated volcanic emissions (Pálfy and Smith, 2000) and igneous intrusions (e.g., Svensen et al., 2007), along with the release of carbon from methane hydrates (Hesselbo et al., 2000), resulted in almost a doubling of the atmospheric pCO_2 levels, leading to an abrupt warming of 7–10°C during the T-OAE (Bailey et al.,

https://doi.org/10.5194/egusphere-2026-2964
Preprint. Discussion started: 21 July 2026

2003; Price, 2010; Ruebsam et al., 2020; Ullmann et al., 2020). This volcanic link is supported by widespread Hg enrichment during the event in several sections (e.g., Percival et al., 2015; Fantasia et al., 2018; Ruhl et al., 2022).

5.4 Environmental disturbance at the CPE compared to other global change events

The CPE is characterized by a suite of environmental changes including the shutdown of carbonate platform productivity (e.g. Hornung et al., 2007; Stefani et al., 2010; Jin et al., 2019), elevated global temperatures (e.g., Hornung et al., 2007; Trotter et al., 2015; Sun et al., 2016), intensification of global weathering (e.g., Rostási et al., 2011; Barrenechea et al., 2018; Zhang et al., 2024a), and increased marine anoxia (e.g., Hornung and Brandner, 2005; Sun et al., 2016; Tomimatsu et al., 2021). An NCIE of ~2–7‰ associated with the CPE, together with synchronous increases in Hg and Hg/TOC concentrations, enhanced siliciclastic influx, elevated kaolinite content, and weathering indices (e.g., Rostási et al., 2011; Zhang et al., 2024), and a concurrent decrease in seawater $^{187}Os/^{188}Os$ ratios (Xu et al., 2014; Tomimatsu et al., 2021), collectively indicate a strong link to volcanism and resulting intensification of chemical weathering processes (Mazaheri-Johari et al., 2021; Lu et al., 2021; Shen et al., 2022; Zhao et al., 2022). The inferred volcanogenic CO_2 injection likely enhanced the hydrological cycle, intensifying weathering and erosion, which in turn introduced siliciclastic deposits that may have smothered carbonate productivity on marginal marine platforms (Rigo et al., 2007; Dal Corso et al., 2015). An enhanced hydrological cycle during the CPE is also indicated by the expansion of fluvial lakes (Ji et al., 2010; Kozur and Bachmann, 2010; Arche and López-Gómez, 2014), a shift to hygrophyte herbage (e.g., Roghi et al., 2010; Baranyi et al., 2019), and increased freshwater algae abundance (Baranyi et al., 2019; Lu et al., 2021). The $\delta^{18}O$ conodont record further indicates locally decreased salinity and warming of up to 7°C (Hornung et al., 2007; Rigo and Joachimski, 2010; Trotter et al., 2015; Sun et al., 2016). The observed negative carbon isotope excursions may reflect either direct CO_2 input into the ocean-atmosphere system or secondary cascade effects triggered by volcanism, such as the release of isotopically lighter carbon from seafloor methane clathrates due to elevated seawater temperatures, thereby explaining the large magnitude of the excursions (Dal Corso et al., 2012; Miller et al., 2017).

Similar to the CPE, the T-OAE is also characterized by a carbonate productivity crisis (Palliani et al., 2002; Tremolada et al., 2005; Mattioli et al., 2009), biotic extinctions and radiations (Harries and Little, 1999; Aberhan and Baumiller, 2003; Tremolada et al., 2005; Danise et al., 2019), increased continental weathering rates of 200–500%, increased storm activity, and higher terrigenous runoff resulting in the occurrence of sandstones, debris-flow deposits and turbidites into deeper marine environments under a wetter and more humid climate regime (Cohen et al., 2004; Hesselbo et al., 2007; Brazier et al., 2015; Fu et al., 2017; Izumi et al., 2018; Them et al., 2017; Fantasia et al., 2018; Kemp et al., 2024). Development and expansion of large lake systems has also been reported to occur contemporaneously with the Toarcian OAE (e.g., Xu et al., 2017; Jin et al., 2020), with the enhanced hydrological cycling driving higher primary productivity, resulting in subsequent oxygen depletion and widespread anoxic conditions, leading to the deposition and preservation of organic-rich black shales not only in marine environments worldwide, but even in major inland lake systems at this time (Jenkyns, 1988; Jenkyns, 2010; Dickson et al., 2017).

https://doi.org/10.5194/egusphere-2026-2964
Preprint. Discussion started: 21 July 2026

Deposition of black shale coeval with the CPE has been reported at multiple locations (Hornung and Brandner, 2005; Wang et al., 2008; Soua, 2014) and attributed to oxygen depletion in the oceans caused by increased nutrient influx due to higher rates of weathering. Anoxia extending to at least basin slopes has also been recorded in the Dolomites of Italy (Keim et al., 2006) and in similar settings in the Indian Himalayas (Hornung et al., 2007). An enrichment of redox-sensitive elements such as vanadium, molybdenum, and uranium in the late Julian also indicates the development or expansion of locally reducing oceanographic conditions (Xu et al., 2014; Tomimatsu et al., 2021).

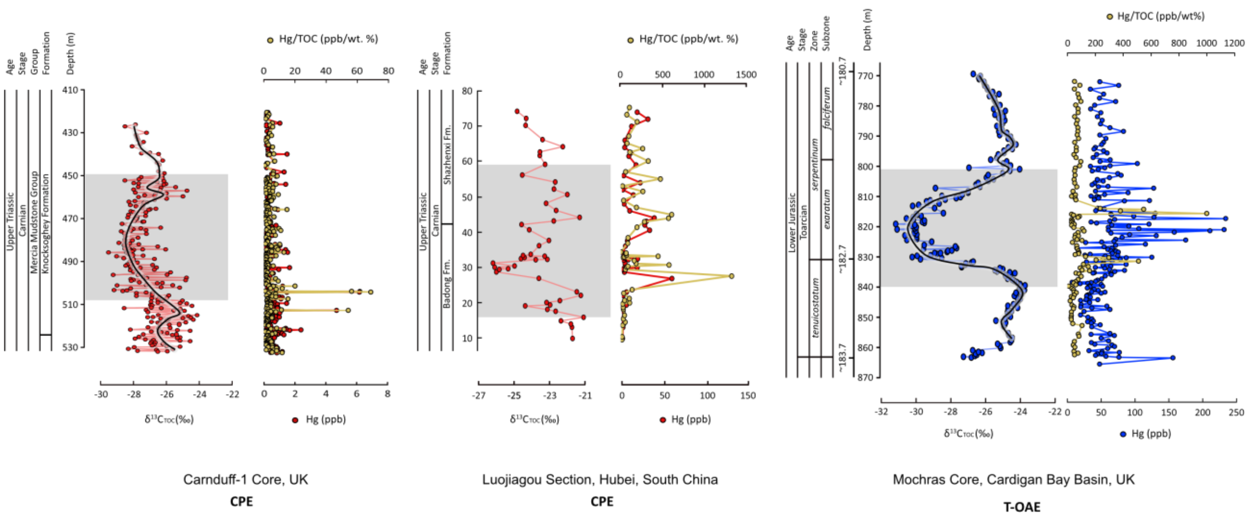

Figure 4: Comparison of $\delta^{13}C_{TOC}$ and Hg records across the CPE interval in the Knocksoghey Formation (This study), and Luojiagou Section, Hubei, South China ($\delta^{13}C_{org}$ from Li et al., 2022) with $\delta^{13}C_{org}$ and Hg records of the Toarcian Oceanic Anoxic Event as recorded in the Mochras Core of the Cardigan Bay Basin, UK (Xu et al., 2018; Ruhl et al., 2022).

The release of light carbon during the T-OAE occurred in a series of discrete, stepped pulses of varying magnitudes (e.g., Kemp et al., 2005), collectively building up to a longer-term negative CIE. The comparison of the CPE with the well-studied carbon-isotope archives spanning the T-OAE highlights the similarity in the $\delta^{13}C$ evolution during other events (Kemp et al., 2005; Hesselbo et al., 2007; Hermoso et al., 2009; Xu et al., 2018). In the geochemical comparison between the $\delta^{13}C_{org}$ and Hg record from this study and the Badong and Shazhenxi Formations in the Luojiagou section, Zigui Basin, Hubei, South China (Li et al., 2022), with the Mochras Core from the Cardigan Bay Basin, UK (Xu et al., 2018), the records exhibit a similar excursion pattern, characterized by a positive trend of ~3–4‰, interrupted by a stepwise decline to negative $\delta^{13}C$ values, followed by a gradual recovery towards heavier values (Fig. 4). Both excursions appear to be symmetrical, with a comparable stepped onset. The Mochras record is also marked by coarser gravity-flow deposits succeeding the excursion onset, similar to the sandstone beds observed in the Knocksoghey Formation. A switch to more humid conditions is also evidenced by the elevated kaolinite to illite ratio coinciding with the onset of the excursion within the Mochras core.

https://doi.org/10.5194/egusphere-2026-2964
Preprint. Discussion started: 21 July 2026

Both events are indeed accompanied by multiple biotic and geochemical changes, including extinctions and major shifts in the distribution of marine and terrestrial species, increased global warming, and higher rates of weathering and runoff. Hence, in terms of their stratigraphic and Earth system appearance, both the CPE and the T-OAE appear to be similar, and possibly also stemming from a similar forcing mechanism with an increased input of $\delta^{13}C$-depleted carbon into the ocean-atmospheric environment.

5.5 Sedimentary mercury (Hg) enrichment during the Carnian Pluvial Episode

Anomalous levels of mercury in sedimentary successions have been attributed to volcanic emissions, and over the years, several studies have shown a positive correlation between stratigraphic spikes in sedimentary Hg levels and past (LIP) volcanic events (e.g., Sanei et al., 2012; Grasby et al., 2013; Percival et al., 2015; Sial et al., 2016; Gong et al., 2017; Ruhl et al., 2020; Ruhl et al., 2022). However, Hg can be sequestered in sediments through multiple processes other than volcanic loading, including Hg enrichment from increased pyrite burial, increased delivery of terrestrial-sourced Hg, or increased clay mineral deposition (e.g., Grasby et al., 2019; Shen et al., 2020; Kovács et al., 2024).

The Hg profile for the Knocksoghey Formation is consistent with the uniformly organic-lean nature of the sediments. Typically, very low sedimentary total organic carbon (TOC) contents can yield spurious Hg/TOC results (Grasby et al., 2019). Given the consistent, fairly low TOC levels in the here studied record, the Hg/TOC trend observed here appears to mirror the stratigraphic record of sedimentary Hg concentrations. Since assessed Hg/TOC values become increasingly meaningless with decreasing sedimentary TOC, and since the TOC values in the here analyzed succession are commonly below the recommended lower limit for TOC normalization (Grasby et al., 2019), absolute sedimentary Hg concentrations are emphasized here. The overall Hg concentrations recorded in the CRN-1 core are almost negligible (averaging 0.3 ppb), and all values are markedly below the mean value reported for clastic sediments (62.4 ppb) (Grasby et al., 2019), exhibiting no significant sustained enrichment as observed in other CPE sections (Mazaheri-Johari et al., 2021; Lu et al., 2021; Zhao et al., 2025) (Fig.5). However, replicate analyses confirm a small, but discrete enrichment in Hg at the onset of the negative carbon isotopic excursion, while TOC levels remain low and unchanged relative to stratigraphically pre- and succeeding samples.

The elevated Hg concentration precedes the siliciclastic input, which eliminates increased runoff as a possible contributor to the observed Hg signal. Hg shows only minor correlation with TOC ($R = 0.11$) and Al ($R = -0.14$), indicating that neither organic matter nor clay mineral composition exerts a dominant source and/or lithological control over Hg concentrations within the samples. In aquatic environments, strong euxinia may promote pyrite formation, which can scavenge Hg (Sanei et al., 2012; Shen et al., 2020). In instances where dissolved sulfates are made available by evaporites such as gypsum or anhydrite, pyrite formation may also be possible in a continental saline-lake setting, such as that of the Knocksoghey Formation. Mercury covariance with Fe is therefore evaluated, in addition to TOC and Al. In this case, Fe concentrations are used as a qualitative indicator of pyrite-hosted Hg, although Fe may be present in variable phases across a sedimentary archive. This approach has been employed previously by multiple authors to account for possible Hg drawdown by Fe-

https://doi.org/10.5194/egusphere-2026-2964
Preprint. Discussion started: 21 July 2026

bearing host phases, including pyrites and/or Fe oxyhydroxides (e.g., Charbonnier et al., 2017; Sabatino et al., 2018; Kalvoda et al., 2019). However, samples from the Knocksoghey Formation exhibit negligible correlation between Hg and Fe ($R = -0.09$), suggesting that Hg concentrations are not tied to Fe and, by extension, possibly not to pyrite either. Instead, the coincidence of the elevated sedimentary Hg levels and the onset of the negative CIE, as also observed in other CPE sections (Fig. 5), suggests the recording of a short-lived, although modest, enhancement of Hg delivery to this continental basin, possibly associated with increased magmatism (such as Wrangellian Terrane LIP emplacement) at that time.

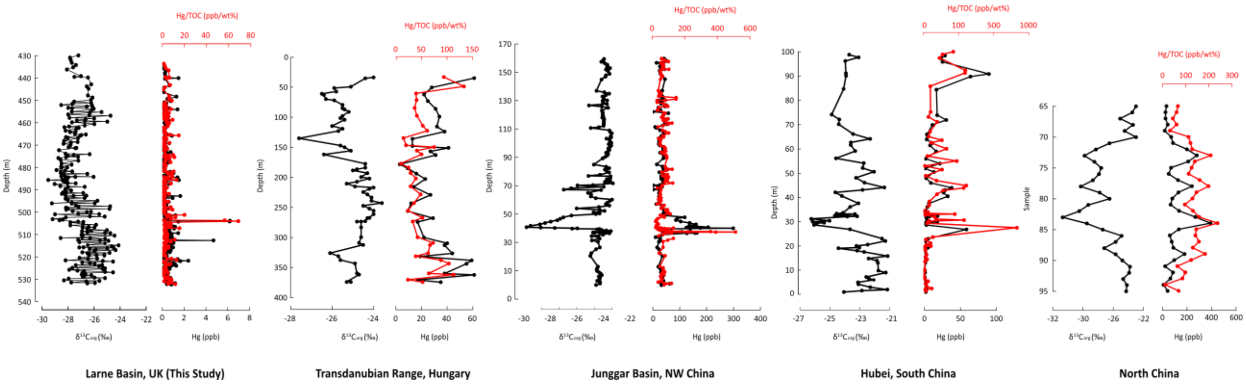

Figure 5: Mercury enrichments coincident with negative $\delta^{13}C_{org}$ excursions in multiple terrestrial and marine sections worldwide. Profiles show Hg (ppb) and Hg/TOC (ppb per wt.%) alongside $\delta^{13}C_{org}$. From left to right, records from: This study; Transdanubian Range (Dal Corso et al., 2015; Mazaheri-Johari et al., 2021); Junggar Basin (Zhao et al., 2025); South China (Li et al., 2022; new Hg/TOC data); North China (Lu et al., 2021).

The Badong Formation from the Luojiagou section in western Hubei, South China, provides an independent and geographically widely separated record of the Carnian Pluvial Episode (CPE). Organic carbon-isotope data from this section (Li et al., 2022) record a stepped negative CIE. Existing stratigraphic and geochronological constraints indicate that the upper Badong Formation extends into the Carnian and preserves a clear CPE-related carbon-cycle perturbation within a terrestrial-marine transitional setting. The new Hg data from the Luojiagou section provide additional geochemical evidence of environmental perturbance within the same interval. Hg and Hg/TOC values show low background levels outside the excursion interval, but sharply increase at the onset of the NCIE. Elevated Hg values continue through the negative excursion, with several pronounced peaks marking discrete episodes of enhanced Hg loading to the basin. Together with the data from the Knocksoghey Formation, the Hg record reveals a clear enrichment in both sections, stratigraphically coincident with the CPE negative carbon isotope excursion. The significantly elevated Hg concentration recorded in the Luojiagou section could be attributed to its paleogeographic position relative to atmospheric transport pathways during the CPE. Modeled wind patterns during the CPE (Zhao et al., 2025) (Fig. 1) suggest that this region may have received enhanced Hg input, potentially contributing to the higher Hg signal observed in the section. The Larne Basin, in contrast, occupied a

https://doi.org/10.5194/egusphere-2026-2964
Preprint. Discussion started: 21 July 2026

palaeogeographic position distal to the main pathways of Wrangellia-derived atmospheric transport, where volcanic Hg loading may have been significantly attenuated.

6 Conclusions

The organic carbon isotope record from the Knocksoghey Formation of the Mercia Mudstone Group in the Larne Basin shows a ~4‰ negative shift in $\delta^{13}C$, synchronous with a modest increase in sedimentary Hg concentrations above background levels. These geochemical changes are followed by an increased pulse of coarse siliciclastics, indicative of enhanced runoff associated with wetter conditions, and then a return to more arid conditions. The geochemical signals that precede the sandy interval are consistent with an external forcing, possibly volcanogenic, that perturbed the carbon cycle before the clastic response of the CPE. The records from the Carnduff-1 core thus imply a short lag between magmatic forcing, climate perturbation, and catchment-to-basin sediment delivery. Elevated CO_2 from coeval magmatism drove wetter conditions and accelerated weathering, rapidly routing coarser quartz-rich sediment to the basin and producing the observed coarsening-upward, event-bed character. The stacked anhydrite series marks a return to increasingly restricted, arid conditions after the pluvial pulse.

The stepped nature of the carbon isotope shift to more negative values and the absence of repeated returns to baseline values until the end of the excursion suggest a pulsed excursion similar to other LIP-driven events in the Phanerozoic (such as the Toarcian Oceanic Anoxic Event). The overall notable similarities between the two events, including the associated sedimentological, biotic, and geochemical changes, as well as the nature and magnitude of the carbon isotopic excursions, support the W-LIP as a driver of the CPE, as evidenced by the correlation of $\delta^{13}C$ and Hg/TOC from a variety of global localities.

Anthropogenically driven climate change has increased the frequency of pluvial events in recent years. These events are expected to become more intense and last longer, with future projections showing that this variation, along with an increase in storm intensity and fluvial sediment loading, is expected to increase globally with significant social and economic impacts (e.g., Pendergrass et al., 2017; IPCC, 2023), with the highest variability and duration expected in the tropics and mid-latitudes (Martin, 2018). With this climatic crisis at hand, identifying and improving our understanding of past events globally that are analogous to the present will enhance predictive models of latitudinal variability in climate and precipitation, including impacts, intensities, feedback mechanisms, and the frequency of similar pluvial events or episodes.

https://doi.org/10.5194/egusphere-2026-2964
Preprint. Discussion started: 21 July 2026

490 **Appendix A**

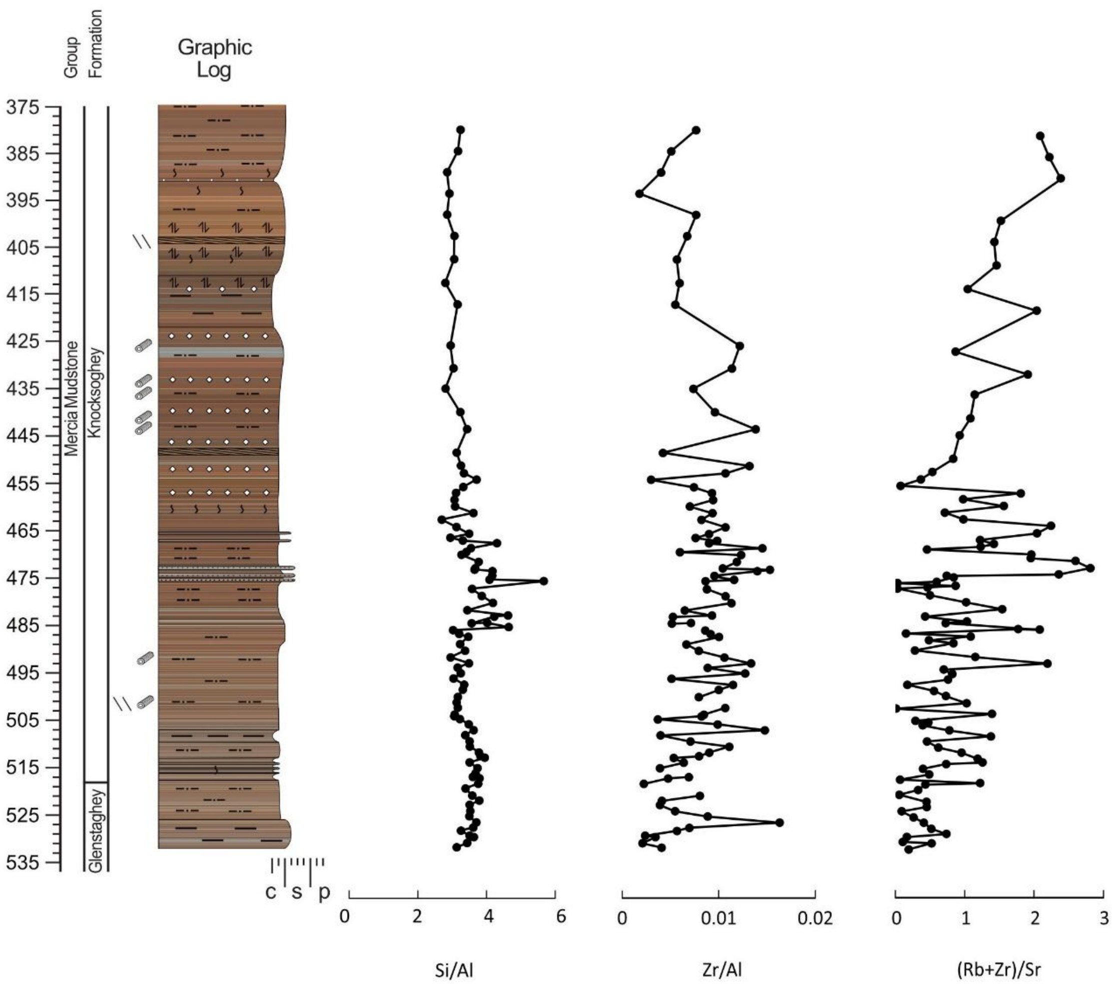

Figure A1: Variation of terrigenous input proxies Si/Al, Zr/Al and (Rb+Zr)/Sr through the studied interval of the Carnduff-1 core. All ratios are plotted against depth and expressed relative to Al and Sr. Higher values of Si/Al and Zr/Al reflect increased siliciclastic influx, whereas elevated (Rb+Zr)/Sr highlights enhanced detrital input relative to carbonate.

https://doi.org/10.5194/egusphere-2026-2964
Preprint. Discussion started: 21 July 2026

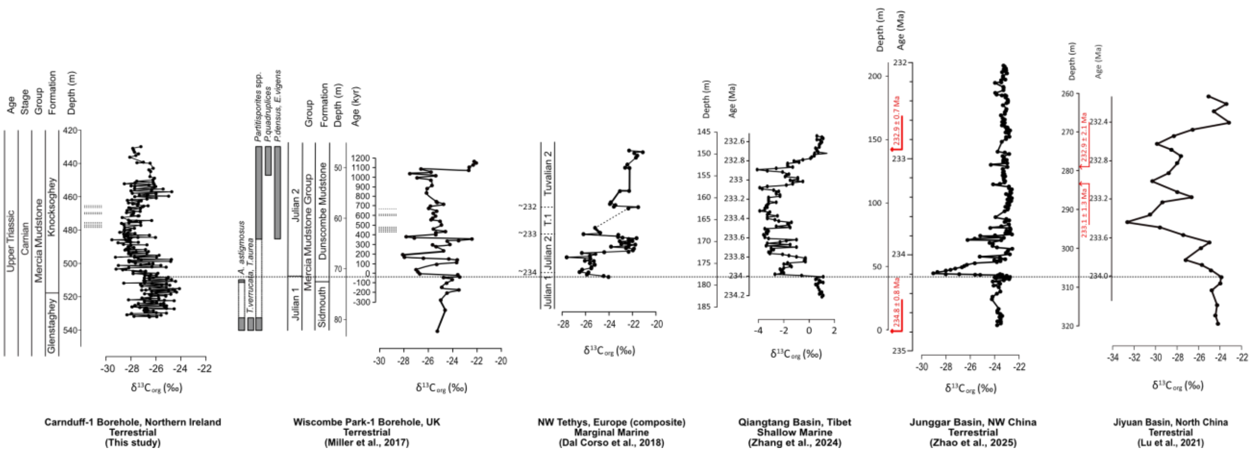

Figure A2: Correlation of data from the Knocksoghey Formation with published δ^{13}C records from terrestrial and marine successions recording the CPE worldwide. The black dotted line indicates the onset of CPE NCIE. Radiometric, astrochronologic, and biostratigraphic controls are shown where available.

Data availability

All data needed to evaluate the conclusions are hosted on the Zenodo data repository and will be made available after publication:10.5281/zenodo.20347975 (Shahid et al., 2026).

Author contributions

The authors contributed to the paper as follows: conceptualization by AAS, MR & MMS; writing the original draft by MMS; investigation by MMS, AAS, MR, AP & YW; formal analysis by MMS; visualization by MMS & AAS; resources by AAS, MR, & RR; data curation by MMS, AAS, FOO & MR; review and editing by AAS, MR & FOO; methodology by AAS; funding acquisition by AAS; supervision by AAS; and project administration by AAS.

Competing interests

The authors declare that they have no conflicts of interest.

Acknowledgements

We thank Vijo Poulose (UAE University) for technical assistance with XRF analysis.

We also acknowledge the use of AI to check spelling, syntax, and typographical errors, and to improve writing clarity. AI was not used for any analysis of data, data interpretation, or other aspects of this manuscript.

Financial support

This project was funded through Khalifa University RIG-S-2023-108 The Carnian Pluvial Episode: An ancient analogue for modern intensification of the hydrological cycle and extreme precipitation events" and funding from the Polar Research Centre.

References

Aberhan, M. and Baumiller, T. K.: Selective extinction among Early Jurassic bivalves; a consequence of anoxia, Geology, 31, 1077–1080, https://doi.org/10.1130/G19938.1, 2003.

Al-Suwaidi, A. H., Angelozzi, G. N., Baudin, F., Damborenea, S. E., Hesselbo, S. P., Jenkyns, H. C., Manceñido, M. O., and Riccardi, A. C.: First record of the Early Toarcian Oceanic Anoxic Event from the Southern Hemisphere, Neuquén Basin, Argentina, J. Geol. Soc., 167, 633–636, https://doi.org/10.1144/0016-76492010-025, 2010.

Andeskie, A. S., Benison, K. C., Eichenlaub, L. A., and Raine, R.: Acid-saline-lake systems of the Triassic Mercia Mudstone Group, County Antrim, Northern Ireland, J. Sediment. Res., 88, 385–398, https://doi.org/10.2110/jsr.2018.14, 2018.

Arche, A. and López-Gómez, J.: The Carnian Pluvial Event in western Europe: new data from Iberia and correlation with the western Neotethys and eastern North America–NW Africa regions, Earth-Sci. Rev., 128, 196–231, https://doi.org/10.1016/j.earscirev.2013.10.012, 2014.

Bailey, T. R., Rosenthal, Y., McArthur, J. M., van de Schootbrugge, B., and Thirlwall, M. F.: Paleoceanographic changes of the late Pliensbachian–Early Toarcian interval: a possible link to the genesis of an Oceanic Anoxic Event, Earth Planet. Sci. Lett., 212, 307–320, https://doi.org/10.1016/S0012-821X(03)00278-4, 2003.

Baranyi, V., Miller, C. S., Ruffell, A., Hounslow, M. W., and Kürschner, W. M.: A continental record of the Carnian Pluvial Episode (CPE) from the Mercia Mudstone Group (UK): palynology and climatic implications, J. Geol. Soc., 176, 149–166, https://doi.org/10.1144/jgs2017-150, 2019.

Baranyi, V., Budai, T., Karádi, V., Jin, X., Kürschner, W. M., and Tóth, E.: Vegetation and climate record across the Carnian Pluvial episode from the Transdanubian Range, Hungary, Western Tethys, Palaeogeogr. Palaeocl., 671, 112989, https://doi.org/10.1016/j.palaeo.2025.112989, 2025.

Barrenechea, J. F., López-Gómez, J., and de la Horra, R.: Sedimentology, clay mineralogy and palaeosols of the mid-Carnian Pluvial Episode in eastern Spain: insights into humidity and sea-level variations, J. Geol. Soc., 175, 993–1003, https://doi.org/10.1144/jgs2018-024, 2018.

Benton, M. J., Bernardi, M., and Kinsella, C.: The Carnian Pluvial Episode and the origin of dinosaurs, J. Geol. Soc., 175, 1019–1026, https://doi.org/10.1144/jgs2018-049, 2018.

Bernardi, M., Gianolla, P., Petti, F. M., Mietto, P., and Benton, M. J.: Dinosaur diversification linked with the Carnian Pluvial Episode, Nat. Commun., 9, 1499, https://doi.org/10.1038/s41467-018-03996-1, 2018.

Bjørlykke, K.: Relationships between depositional environments, burial history and rock properties: some principal aspects of diagenetic processes in sedimentary basins, Sediment. Geol., 301, 1–14, https://doi.org/10.1016/j.sedgeo.2013.12.002, 2014.

Boomer, I., Copestake, P., Raine, R., Azmi, A., Fenton, J. P. G., Page, K. N., and O'Callaghan, M.: Stratigraphy, palaeoenvironments and geochemistry across the Triassic–Jurassic Boundary transition at Carnduff, County Antrim, Northern Ireland, Proc. Geol. Assoc., 132, 667–687, https://doi.org/10.1016/j.pgeola.2020.05.004, 2021.

Boulvain, F., Belanger, I., Delsate, D., Ghysel, P., Godefroit, P., Laloux, M., Monteyne, R., and Roche, M.: Triassic and Jurassic lithostratigraphic units (Belgian Lorraine), Geol. Belg., 4, 113–119, https://hdl.handle.net/2268/18985, 2001.

Brazier, J., Suan, G., Tacail, T., Simon, L., Martin, J. E., Mattioli, E., and Balter, V.: Calcium isotope evidence for a dramatic increase in continental weathering during the Toarcian Oceanic Anoxic Event (Early Jurassic), Earth Planet. Sci. Lett., 411, 164–176, https://doi.org/10.1016/j.epsl.2014.11.028, 2015.

Palliani, R. B., Mattioli, E., and Riding, J. B.: The response of marine phytoplankton and sedimentary organic matter to the Early Toarcian (Lower Jurassic) Oceanic Anoxic Event in Northern England, Mar. Micropaleontol., 46, 223–245, https://doi.org/10.1016/S0377-8398(02)00064-6, 2002.

Buggle, B., Glaser, B., Hambach, U., Gerasimenko, N., and Marković, S.: An evaluation of geochemical weathering indices in loess–paleosol studies, Quatern. Int., 240, 12–21, https://doi.org/10.1016/j.quaint.2010.07.019, 2011.

Callegaro, S., Dal Corso, J., and Song, H.: How large igneous provinces (LIPs) during the Triassic shaped modern-day ecosystems, Front. Earth Sci., 11, 1302216, https://doi.org/10.3389/feart.2023.1302216, 2023.

Charbonnier, G., Morales, C., Duchamp-Alphonse, S., Westermann, S., Adatte, T., and Föllmi, K. B.: Mercury enrichment indicates volcanic triggering of Valanginian environmental change, Sci. Rep., 7, 40808, https://doi.org/10.1038/srep40808, 2017.

Cohen, A. S., Coe, A. L., Harding, S. M., and Schwark, L.: Osmium isotope evidence for the regulation of atmospheric CO2 by continental weathering, Geology, 32, 157–160, https://doi.org/10.1130/G20158.1, 2004.

Cooper, M. R., Schofield, D., Haslam, R., Wilson, P., Lewis, M., Bloomfield, J. P., Lee, J. R., Baptie, B., Shaw, R. P., Reay, D. M., Bide, T., and McEvoy, F. M.: National Geological Screening: Northern Ireland, British Geological Survey Commissioned Report, CR/17/096, 72 pp., 2018.

Dal Corso, J., Mietto, P., Newton, R. J., Pancost, R. D., Preto, N., Roghi, G., and Wignall, P. B.: Discovery of a major negative ^{13}C spike in the Carnian (Late Triassic) linked to the eruption of Wrangellia flood basalts, *Geology*, 40, 79–82, https://doi.org/10.1130/G32473.1, 2012.

Dal Corso, J., Gianolla, P., Newton, R. J., Franceschi, M., Roghi, G., Caggiati, M., Raucsik, B., Budai, T., Haas, J., and Preto, N.: Carbon isotope records reveal synchronicity between carbon cycle perturbation and the "Carnian Pluvial Event" in the Tethys realm (Late Triassic), Global Planet. Change, 127, 79–90, https://doi.org/10.1016/j.gloplacha.2015.01.013, 2015.

Dal Corso, J., Gianolla, P., Rigo, M., Franceschi, M., Roghi, G., Mietto, P., Manfrin, S., Raucsik, B., Budai, T., Jenkyns, H. C., and Reymond, C. E.: Multiple negative carbon-isotope excursions during the Carnian Pluvial Episode (Late Triassic), Earth-Sci. Rev., 185, 732–750, https://doi.org/10.1016/j.earscirev.2018.07.004, 2018.

Danise, S., Clémence, M. E., Price, G. D., Murphy, D. P., Gómez, J. J., and Twitchett, R. J.: Stratigraphic and environmental control on marine benthic community change through the early Toarcian extinction event (Iberian Range, Spain), Palaeogeogr. Palaeocl., 524, 183–200, https://doi.org/10.1016/j.palaeo.2019.03.039, 2019.

Dal Corso, J., Bernardi, M., Sun, Y., Song, H., Seyfullah, L. J., Preto, N., Gianolla, P., Ruffell, A., Kustatscher, E., Roghi, G., and Merico, A.: Extinction and dawn of the modern world in the Carnian (Late Triassic), Sci. Adv., 6, eaba0099, https://doi.org/10.1126/sciadv.aba0099, 2020.

Datta, P. M.: Earliest mammal with transversely expanded upper molar from the Late Triassic (Carnian) Tiki Formation, South Rewa Gondwana Basin, India, J. Vertebr. Paleontol., 25, 200–207, https://doi.org/10.1671/0272-4634(2005)025[0200:EMWTEU]2.0.CO;2, 2005.

Dickson, A. J., Gill, B. C., Ruhl, M., Jenkyns, H. C., Porcelli, D., Idiz, E., Lyons, T. W., and van den Boorn, S. H. J. M.: Molybdenum-isotope chemostratigraphy and paleoceanography of the Toarcian Oceanic Anoxic Event (Early Jurassic), Paleoceanography, 32, 813–829, https://doi.org/10.1002/2016PA003048, 2017.

English, K. L., English, J. M., Moscardini, R., Haughton, P. D. W., Raine, R. J., and Cooper, M.: Review of Triassic Sherwood Sandstone Group reservoirs of Ireland and Great Britain and their future role in geoenergy applications, Geoenergy, 2, Geoenergy2023-042, https://doi.org/10.1144/geoenergy2023-042, 2024.

Fantasia, A., Föllmi, K. B., Adatte, T., Spangenberg, J. E., and Montero-Serrano, J.: The Early Toarcian Oceanic Anoxic Event: paleoenvironmental and paleoclimatic change across the Alpine Tethys (Switzerland), Global Planet. Change, 162, 53–68, https://doi.org/10.1016/j.gloplacha.2018.01.008, 2018.

Fischer, T. C., Sonibare, O. O., Aschauer, B., Kleine-Benne, E., Braun, P., and Meller, B.: Amber from the Alpine Triassic of Lunz (Carnian, Austria): a classic palaeobotanical site, Palaeontology, 60, 743–759, https://doi.org/10.1111/pala.12313, 2017.

Fu, X., Wang, J., Zeng, S., Feng, X., Wang, D., and Song, C.: Continental weathering and palaeoclimatic changes through the onset of the early Toarcian oceanic anoxic event in the Qiangtang Basin, Eastern Tethys, Palaeogeogr. Palaeocl., 487, 241–250, https://doi.org/10.1016/j.palaeo.2017.09.005, 2017.

Gallois, R. W. and Porter, R. J.: The stratigraphy and sedimentology of the Dunscombe Mudstone Formation (late Triassic) of south-west England, Geoscience in South-West England, 11, 174–182, https://nora.nerc.ac.uk/id/eprint/3786, 2006.

Gallois, R. W.: The stratigraphy of the Mercia Mudstone Group succession (mid- to late Triassic) proved in the Wiscombe Park boreholes, Devon, Geoscience in South-West England, 11, 280–286, https://nora.nerc.ac.uk/id/eprint/4850, 2008.

Gong, Q., Wang, X., Zhao, L., Grasby, S. E., Chen, Z., Zhang, L., Li, Y., Cao, L., and Li, Z.: Mercury spikes suggest volcanic driver of the Ordovician–Silurian mass extinction, Sci. Rep., 7, 5304, https://doi.org/10.1038/s41598-017-05524-5, 2017.

Grasby, S. E., Sanei, H., Beauchamp, B., and Chen, Z.: Mercury deposition through the Permo–Triassic biotic crisis, Chem. Geol., 351, 209–216, https://doi.org/10.1016/j.chemgeo.2013.05.022, 2013.

Grasby, S. E., Them, T. R., Chen, Z., Yin, R., and Ardakani, O. H.: Mercury as a proxy for volcanic emissions in the geologic record, *Earth-Sci. Rev.*, 196, 102880, https://doi.org/10.1016/j.earscirev.2019.102880, 2019.

Harries, P. J. and Little, C. T. S.: The Early Toarcian (Early Jurassic) and the Cenomanian–Turonian (Late Cretaceous) mass extinctions: similarities and contrasts, Palaeogeogr. Palaeocl., 154, 39–66, https://doi.org/10.1016/S0031-0182(99)00086-3, 1999.

Hermoso, M., Le Callonnec, L., Minoletti, F., Renard, M., and Hesselbo, S. P.: Expression of the Early Toarcian negative carbon-isotope excursion in separated carbonate microfractions (Jurassic, Paris Basin), Earth Planet. Sci. Lett., 277, 194–203, https://doi.org/10.1016/j.epsl.2008.10.013, 2009.

Hesselbo, S. P., Gröcke, D. R., Jenkyns, H. C., Bjerrum, C. J., Farrimond, P., Morgans Bell, H. S., and Green, O. R.: Massive dissociation of gas hydrate during a Jurassic oceanic anoxic event, Nature, 406, 392–395, https://doi.org/10.1038/35019044, 2000.

Hesselbo, S. P., Jenkyns, H. C., Duarte, L. V., and Oliveira, L. C. V.: Carbon-isotope record of the early Jurassic (Toarcian) oceanic anoxic event from fossil wood and marine carbonate (Lusitanian Basin, Portugal), Earth Planet. Sci. Lett., 253, 455–470, https://doi.org/10.1016/j.epsl.2006.11.009, 2007.

Hornung, T. and Brandner, R.: Biochronostratigraphy of the Reingraben Turnover (Hallstatt Facies Belt): local black shale events controlled by regional tectonics, climatic change and plate tectonics, Facies, 51, 460–479, https://doi.org/10.1007/s10347-005-0061-x, 2005.

Hornung, T., Krystyn, L., and Brandner, R.: A Tethys-wide mid-Carnian (Upper Triassic) carbonate productivity crisis: evidence for the Alpine Reingraben Event from Spiti (Indian Himalaya)?, J. Asian Earth Sci., 30, 285–302, https://doi.org/10.1016/j.jseaes.2006.10.001, 2007.

Hounslow, M. W. and Gallois, R. W.: Magnetostratigraphy of the Mercia Mudstone Group (Devon, UK): implications for middle to late Triassic magnetic polarity timescales, J. Geol. Soc., 180, jgs2022-173, https://doi.org/10.1144/jgs2022-173, 2023.

Howard, A. S., Warrington, G., Ambrose, K., and Rees, J. G.: A formational framework for the Mercia Mudstone Group (Triassic) of England and Wales, British Geological Survey Research Report, RR/08/04, British Geological Survey, Keyworth, Nottingham, UK, 33 pp., 2008.

IPCC: Climate Change 2021: The Physical Science Basis: Working Group I Contribution to the Sixth Assessment Report of the Intergovernmental Panel on Climate Change, Cambridge University Press, Cambridge, UK and New York, NY, USA, https://doi.org/10.1017/9781009157896, 2023.

Izumi, K., Kemp, D. B., Itamiya, S., and Inui, M.: Sedimentary evidence for enhanced hydrological cycling in response to rapid carbon release during the early Toarcian oceanic anoxic event, Earth Planet. Sci. Lett., 481, 162–170, https://doi.org/10.1016/j.epsl.2017.10.030, 2018.

Jenkyns, H. C.: The Early Toarcian (Jurassic) Anoxic Event: stratigraphic, sedimentary, and geochemical evidence, Am. J. Sci., 288, 101–151, https://doi.org/10.2475/ajs.288.2.101, 1988.

Jenkyns, H. C.: Geochemistry of oceanic anoxic events, Geochem. Geophys. Geosyst., 11, Q03004, https://doi.org/10.1029/2009GC002788, 2010.

Jeram, A. J., Simms, M. J., Hesselbo, S. P., and Raine, R.: Carbon isotopes, ammonites and earthquakes: key Triassic-Jurassic boundary events in the coastal sections of south-east County Antrim, Northern Ireland, UK, Proc. Geol. Assoc., 132, 702–725, https://doi.org/10.1016/j.pgeola.2021.10.004, 2021.

Ji, L., Yan, K., Meng, F., and Zhao, M.: The oleaginous Botryococcus from the Triassic Yanchang Formation in Ordos Basin, Northwestern China: morphology and its paleoenvironmental significance, J. Asian Earth Sci., 38, 175–185, https://doi.org/10.1016/j.jseaes.2009.12.010, 2010.

Jin, X., McRoberts, C., Shi, Z., Mietto, P., Rigo, M., Roghi, G., Manfrin, S., Franceschi, M., and Preto, N.: The aftermath of the CPE and the Carnian–Norian transition in the northwestern Sichuan Basin, South China, J. Geol. Soc., 176, 179–196, https://doi.org/10.1144/jgs2018-104, 2019.

Jin, X., Shi, Z., Baranyi, V., Kemp, D. B., Han, Z., Luo, G., Hu, J., He, F., Chen, L., and Preto, N.: The Jenkyns Event (Early Toarcian OAE) in the Ordos Basin, North China, Global Planet. Change, 193, 103273, https://doi.org/10.1016/j.gloplacha.2020.103273, 2020.

Kafousia, N., Karakitsios, V., Mattioli, E., Kenjo, S., and Jenkyns, H. C.: The Toarcian Oceanic Anoxic Event in the Ionian Zone, Greece, Palaeogeogr. Palaeocl., 393, 135–145, https://doi.org/10.1016/j.palaeo.2013.11.013, 2014.

Kalvoda, J., Kumpan, T., Qie, W., Frýda, J., and Bábek, O.: Mercury spikes at the Devonian–Carboniferous boundary in the eastern part of the Rhenohercynian Zone (central Europe) and in the South China Block, Palaeogeogr. Palaeocl., 531, 109221, https://doi.org/10.1016/j.palaeo.2019.109221, 2019.

Keim, L., Spötl, C., and Brandner, R.: The aftermath of the Carnian carbonate platform demise: a basinal perspective (Dolomites, Southern Alps), Sedimentology, 53, 361–386, https://doi.org/10.1111/j.1365-3091.2006.00768.x, 2006.

Kemp, D. B., Coe, A. L., Cohen, A. S., and Schwark, L.: Astronomical pacing of methane release in the Early Jurassic period, Nature, 437, 396–399, https://doi.org/10.1038/nature04037, 2005.

Kemp, D. B., Han, Z., Hu, X., Chen, W., Jin, S., Izumi, K., Yan, Q., Baranyi, V., Jin, X., Dal Corso, J., and Ge, Y.: Global hydroclimate perturbations during the Toarcian Oceanic Anoxic Event, Earth-Sci. Rev., 258, 104946, https://doi.org/10.1016/j.earscirev.2024.104946, 2024.

Korte, C., Kozur, H. W., and Veizer, J.: $\delta^{13}C$ and $\delta^{18}O$ values of Triassic brachiopods and carbonate rocks as proxies for coeval seawater and palaeotemperature, Palaeogeogr. Palaeocl., 226, 287–306, https://doi.org/10.1016/j.palaeo.2005.05.018, 2005.

Kovács, E. B., Ruhl, M., Silva, R. L., McElwain, J. C., Reolid, M., Korte, C., Ruebsam, W., and Hesselbo, S. P.: Mercury sequestration pathways under varying depositional conditions during Early Jurassic (Pliensbachian and Toarcian) Karoo–Ferrar volcanism, Palaeogeogr. Palaeocl., 637, 111977, https://doi.org/10.1016/j.palaeo.2023.111977, 2024.

Kozur, H. W. and Bachmann, G. H.: The Middle Carnian wet intermezzo of the Stuttgart Formation (Schilfsandstein), Germanic Basin, Palaeogeogr. Palaeocl., 290, 107–119, https://doi.org/10.1016/j.palaeo.2009.11.004, 2010.

Lecuona, A., Ezcurra, M. D., and Irmis, R. B.: Revision of the early crocodylomorph *Trialestes romeri* (Archosauria, Suchia) from the lower Upper Triassic Ischigualasto Formation of Argentina: one of the oldest-known crocodylomorphs, Pap. Palaeontol., 2, 585–622, https://doi.org/10.1002/spp2.1056, 2016.

Lestari, W., Al-Suwaidi, A., Fox, C. P., Vajda, V., and Hennhoefer, D.: Carbon cycle perturbations and environmental change of the Middle Permian and Late Triassic Paleo-Antarctic Circle, Sci. Rep., 14, 9742, https://doi.org/10.1038/s41598-024-60088-5, 2024.

Li, Q., Ruhl, M., Wang, Y. D., Xie, X. P., An, P. C., and Xu, Y. Y.: Response of Carnian Pluvial Episode evidenced by organic carbon isotopic excursions from western Hubei, South China, Palaeoworld, 31, 324–333, https://doi.org/10.1016/j.palwor.2021.08.004, 2022.

Lu, J., Zhang, P., Dal Corso, J., Yang, M., Wignall, P. B., Greene, S. E., Shao, L., Lyu, D., and Hilton, J.: Volcanically driven lacustrine ecosystem changes during the Carnian Pluvial Episode (Late Triassic), Proc. Natl. Acad. Sci. U.S.A., 118, e2109895118, https://doi.org/10.1073/pnas.2109895118, 2021.

Mancuso, A. C., Benavente, C. A., Irmis, R. B., and Mundil, R.: Evidence for the Carnian Pluvial Episode in Gondwana: new multiproxy climate records and their bearing on early dinosaur diversification, Gondwana Res., 86, 104–125, https://doi.org/10.1016/j.gr.2020.05.009, 2020.

Mansour, A., Gentzis, T., Ied, I. M., Ahmed, M. S., and Wagreich, M.: Paleoenvironmental conditions and factors controlling organic carbon accumulation during the Jurassic–Early Cretaceous, Egypt: organic and inorganic geochemical approach, Minerals, 12, 1213, https://doi.org/10.3390/min12101213, 2022.

Mao, X., Liu, X., and Zhou, X.: Permo-Triassic aeolian red clay of southwestern England and its palaeoenvironmental implications, Aeolian Res., 52, 100726, https://doi.org/10.1016/j.aeolia.2021.100726, 2021.

Martin, E. R.: Future projections of global pluvial and drought event characteristics, Geophys. Res. Lett., 45, 11913–11920, https://doi.org/10.1029/2018GL079807, 2018.

Matschullat, J., Ottenstein, R., and Reimann, C.: Geochemical background: can we calculate it?, Environ. Geol., 39, 990–1000, https://doi.org/10.1007/s002549900084, 2000.

Mattioli, E., Pittet, B., Petitpierre, L., and Mailliot, S.: Dramatic decrease of pelagic carbonate production by nannoplankton across the early Toarcian anoxic event (T-OAE), Global Planet. Change, 65, 134–145, https://doi.org/10.1016/j.gloplacha.2008.10.018, 2009.

Mazaheri-Johari, M., Gianolla, P., Mather, T. A., Frieling, J., Chu, D., and Dal Corso, J.: Mercury deposition in Western Tethys during the Carnian Pluvial Episode (Late Triassic), Sci. Rep., 11, 17339, https://doi.org/10.1038/s41598-021-96890-8, 2021.

Merlin Energy Resources Consortium: The Standard Stratigraphic Nomenclature of Offshore Ireland: An Integrated Lithostratigraphic, Biostratigraphic and Sequence Stratigraphic Framework, Project Atlas, Petroleum Affairs Division, Department of Communications, Climate Action and Environment, Special Publication 1/21, 2020.

Miller, C. S., Peterse, F., Da Silva, A. C., Baranyi, V., Reichart, G. J., and Kürschner, W. M.: Astronomical age constraints and extinction mechanisms of the Late Triassic Carnian crisis, Sci. Rep., 7, 2557, https://doi.org/10.1038/s41598-017-02817-7, 2017.

Mitchell, W. I.: Triassic, in: The Geology of Northern Ireland: Our Natural Foundation, 2nd edn., edited by: Mitchell, W. I., Geological Survey of Northern Ireland, Belfast, 133–144, 2004.

Mueller, S., Hounslow, M. W., and Kürschner, W. M.: Integrated stratigraphy and palaeoclimate history of the Carnian Pluvial Event in the Boreal realm: new data from the Upper Triassic Kapp Toscana Group in central Spitsbergen, Norway, J. Geol. Soc., 173, 186–202, https://doi.org/10.1144/jgs2015-028, 2016.

Nesbitt, S. J., Butler, R. J., Ezcurra, M. D., Barrett, P. M., Stocker, M. R., Angielczyk, K. D., Smith, R. M., Sidor, C. A., Niedźwiedzki, G., Sennikov, A. G., and Charig, A. J.: The earliest bird-line archosaurs and the assembly of the dinosaur body plan, Nature, 544, 484–487, https://doi.org/10.1038/nature22037, 2017.

Pálfy, J. and Smith, P. L.: Synchrony between Early Jurassic extinction, oceanic anoxic event, and the Karoo–Ferrar flood basalt volcanism, Geology, 28, 747–750, https://doi.org/10.1130/0091-7613(2000)28%3C747:SBEJEO%3E2.0.CO;2, 2000.

Pedernera, T. E., Irmis, R. B., and Mancuso, A. C.: Geochemical insights into Triassic plant fossils from western Gondwana (Argentina): interpreting diagenetic and δ^{13}Corg variability, Palaeogeogr. Palaeocl., 681, 113372, https://doi.org/10.1016/j.palaeo.2025.113372, 2026.

Pendergrass, A. G., Knutti, R., Lehner, F., Deser, C., and Sanderson, B. M.: Precipitation variability increases in a warmer climate, Sci. Rep., 7, 17966, https://doi.org/10.1038/s41598-017-17966-y, 2017.

Penn, I. E., Holliday, D. W., Kirby, G. A., Kubala, M., Sobey, R. A., Mitchell, W. I., Harrison, R. K., and Beckinsale, R. D.: The Larne No. 2 Borehole: discovery of a new Permian volcanic centre, Scott. J. Geol., 19, 333–346, 1983.

Percival, L. M. E., Witt, M. L. I., Mather, T. A., Hermoso, M., Jenkyns, H. C., Hesselbo, S. P., Al-Suwaidi, A. H., Storm, M. S., Xu, W., and Ruhl, M.: Globally enhanced mercury deposition during the end-Pliensbachian extinction and Toarcian OAE: a link to the Karoo–Ferrar large igneous province, Earth Planet. Sci. Lett., 428, 267–280, https://doi.org/10.1016/j.epsl.2015.06.064, 2015.

Preto, N., Willems, H., Guaiumi, C., and Westphal, H.: Erratum to: Onset of significant pelagic carbonate accumulation after the Carnian Pluvial Event (CPE) in the western Tethys, Facies, 60, 907, https://doi.org/10.1007/s10347-012-0338-9, 2014.

Price, G. D.: Carbon-isotope stratigraphy and temperature change during the Early–Middle Jurassic (Toarcian–Aalenian), Raasay, Scotland, UK, Palaeogeogr. Palaeocl., 285, 255–263, https://doi.org/10.1016/j.palaeo.2009.11.018, 2010.

Price, J. R. and Velbel, M. A.: Chemical weathering indices applied to weathering profiles developed on heterogeneous felsic metamorphic parent rocks, Chem. Geol., 202, 397–416, https://doi.org/10.1016/j.chemgeo.2002.11.001, 2003.

Rahman, N. U., Xian, B., Fang, L., Chen, S., Chen, P., Ullah, Z., and Wang, P.: Volcanically driven terrestrial environmental perturbations during the Carnian Pluvial Episode in the Eastern Tethys, Acta Geol. Sin.-Engl., 98, 753–770, https://doi.org/10.1111/1755-6724.15167, 2024.

Raine, R., Fenton, J. P. G., Boomer, I., Azmi, A., and Copestake, P.: Uppermost Triassic to lower Jurassic stratigraphy in the Lough Foyle Basin of County Londonderry, Northern Ireland, Proc. Geol. Assoc., 132, 641–656, https://doi.org/10.1016/j.pgeola.2021.09.007, 2021.

Ratcliffe, K., Wright, M., and Spain, D.: Unconventional methods for unconventional plays: using elemental data to understand shale resource plays, PESA News, 116, 89–93, 2012.

Retallack, G. J., Veevers, J. J., and Morante, R.: Global coal gap between Permian–Triassic extinction and Middle Triassic recovery of peat-forming plants, Geol. Soc. Am. Bull., 108, 195–207, https://doi.org/10.1130/0016-7606(1996)108%3C0195:GCGBPT%3E2.3.CO;2, 1996.

Rigo, M. and Joachimski, M. M.: Palaeoecology of Late Triassic conodonts: constraints from oxygen isotopes in biogenic apatite, Acta Palaeontol. Pol., 55, 471–478, https://doi.org/10.4202/app.2009.0100, 2010.

Rigo, M., Preto, N., Roghi, G., Tateo, F., and Mietto, P.: A rise in the carbonate compensation depth of western Tethys in the Carnian (Late Triassic): deep-water evidence for the Carnian Pluvial Event, Palaeogeogr. Palaeocl., 246, 188–205, https://doi.org/10.1016/j.palaeo.2006.09.013, 2007.

Roghi, G., Gianolla, P., Minarelli, L., Pilati, C., and Preto, N.: Palynological correlation of Carnian humid pulses throughout western Tethys, Palaeogeogr. Palaeocl., 290, 89–106, https://doi.org/10.1016/j.palaeo.2009.11.006, 2010.

Rostási, Á., Raucsik, B., and Varga, A.: Palaeoenvironmental controls on the clay mineralogy of Carnian sections from the Transdanubian Range, Hungary, Palaeogeogr. Palaeocl., 300, 101–112, https://doi.org/10.1016/j.palaeo.2010.12.013, 2011.

Ruebsam, W., Reolid, M., and Schwark, L.: $\delta^{13}C$ of terrestrial vegetation records Toarcian CO_2 and climate gradients, Sci. Rep., 10, 117, https://doi.org/10.1038/s41598-019-56710-6, 2020.

Ruffell, A., Simms, M. J., and Wignall, P. B.: The Carnian Humid Episode of the Late Triassic: a review, Geol. Mag., 153, 271–284, https://doi.org/10.1017/S0016756815000424, 2016.

Ruffell, A. and Kürschner, W. M.: Sediment cyclicity and the Carnian Pluvial Episode: evidence from spectral gamma-ray logging of the Mercia Mudstone Group, SW England, Boletín Geológico y Minero, 131, 231–242, https://doi.org/10.21701/bolgeomin.131.2.002, 2020.

Ruhl, M., Hesselbo, S. P., Al-Suwaidi, A., Jenkyns, H. C., Damborenea, S. E., Manceñido, M. O., and Riccardi, A. C.: On the onset of Central Atlantic Magmatic Province (CAMP) volcanism and environmental and carbon-cycle change at the Triassic–Jurassic transition, Neuquén Basin, Argentina, Earth-Sci. Rev., 208, 103229, https://doi.org/10.1016/j.earscirev.2020.103229, 2020.

Ruhl, M., Hesselbo, S. P., Jenkyns, H. C., Xu, W., Silva, R. L., Matthews, K. J., Mather, T. A., Mac Niocaill, C., and Riding, J. B.: Reduced plate motion controlled timing of Early Jurassic Karoo–Ferrar large igneous province volcanism, Sci. Adv., 8, eabo0866, https://doi.org/10.1126/sciadv.abo0866, 2022.

Sabatino, N., Ferraro, S., Coccioni, R., Bonsignore, M., Del Core, M., Tancredi, V., and Sprovieri, M.: Mercury anomalies in upper Aptian–Lower Albian sediments from the Tethys realm, Palaeogeogr. Palaeocl., 495, 163–170, https://doi.org/10.1016/j.palaeo.2018.01.019, 2018.

Salisbury, J., Gröcke, D. R., McKie, T., Cheung, H. D. R. A., and Raine, R.: Sulfur isotope ($\delta^{34}S$) stratigraphy of evaporites: Application to the UK Triassic, Earth-Sci. Rev., 266, 105130, https://doi.org/10.1016/j.earscirev.2025.105130, 2025.

Sanei, H., Grasby, S. E., and Beauchamp, B.: Latest Permian mercury anomalies, Geology, 40, 63–66, https://doi.org/10.1130/G32596.1, 2012.

Scotese, C. R.: Map folio 45, Late Triassic (Carnian, 222.6 Ma), PALEOMAP Project, https://doi.org/10.13140/2.1.2412.8802, 2013.

Seyfullah, L. J., Roghi, G., Dal Corso, J., and Schmidt, A. R.: The Carnian Pluvial Episode and the first global appearance of amber, J. Geol. Soc., 175, 1012–1018, https://doi.org/10.1144/jgs2017-143, 2018.

Shelton, R.: Tectonic evolution of the Larne Basin, Geol. Soc. Lond. Spec. Publ., 124, 113–133, https://doi.org/10.1144/GSL.SP.1997.124.01.08, 1997.

Shahid, M., Al Suwaidi, A., Ossa, F., Ruhl, M., Perera, A., Raine, R., Wang, Y., and Li, Q.: Carbon Cycle Perturbance During the Carnian Pluvial Episode (Larne Basin, Northern Ireland), V1, Zenodo [data set], 10.5281/zenodo.20347975, 2026.

Shen, J., Feng, Q., Algeo, T. J., Liu, J., Zhou, C., Wei, W., and Chen, J.: Sedimentary host phases of mercury (Hg) and implications for use of Hg as a volcanic proxy, Earth Planet. Sci. Lett., 543, 116333, https://doi.org/10.1016/j.epsl.2020.116333, 2020.

Shen, J., Yin, R., Zhang, S., Algeo, T. J., Bottjer, D. J., Yu, J., O'Connell, B., Planavsky, N. J., Zhou, L., and Anbar, A. D.: Intensified continental chemical weathering and carbon-cycle perturbations linked to volcanism during the Triassic–Jurassic transition, *Nat. Commun.*, 13, 299, https://doi.org/10.1038/s41467-022-27965-x, 2022.

Sial, A. N., Chen, J., Lacerda, L. D., Frei, R., Tewari, V. C., Pandit, M. K., Gaucher, C., Ferreira, V. P., Cirilli, S., Peralta, S., Korte, C., and Barbosa, J. A.: Mercury enrichment and Hg isotopes in Cretaceous–Paleogene boundary successions: links to volcanism and palaeoenvironmental impacts, *Cretac. Res.*, 66, 60–81, https://doi.org/10.1016/j.cretres.2016.05.006, 2016.

Simms, M. J. and Ruffell, A. H.: Synchroneity of climatic change and extinctions in the Late Triassic, Geology, 17, 265–268, https://doi.org/10.1130/0091-7613(1989)017%3C0265:SOCCAE%3E2.3.CO;2, 1989.

Simms, M. J. and Ruffell, A. H.: Climatic and biotic change in the Late Triassic, J. Geol. Soc., 147, 321–327, https://doi.org/10.1144/gsjgs.147.2.0321, 1990.

Simms, M. J. and Ruffell, A. H.: The Carnian Pluvial Episode: from discovery, through obscurity, to acceptance, J. Geol. Soc., 175, 989–992, https://doi.org/10.1144/jgs2018-020, 2018.

Simms, M. J.: Permian and Mesozoic, in: The Geology of Ireland, 2nd edn., edited by: Holland, C. H. and Sanders, I. S., Dunedin Academic Press, Edinburgh, 311–332, 2009.

Soua, M.: Early Carnian anoxic event as recorded in the southern Tethyan margin, Tunisia: an overview, Int. Geol. Rev., 56, 1884–1905, https://doi.org/10.1080/00206814.2014.967315, 2014.

Stefani, M., Furin, S., and Gianolla, P.: The changing climate framework and depositional dynamics of Triassic carbonate platforms from the Dolomites, Palaeogeogr. Palaeocl., 290, 43–57, https://doi.org/10.1016/j.palaeo.2010.02.018, 2010.

Sun, Y. D., Wignall, P. B., Joachimski, M. M., Bond, D. P. G., Grasby, S. E., Lai, X. L., Wang, L.N., Zhang, Z.T., and Sun, S.: Climate warming, euxinia and carbon isotope perturbations during the Carnian (Triassic) crisis in South China, Earth Planet. Sci. Lett., 444, 88–100, https://doi.org/10.1016/j.epsl.2016.03.037, 2016.

Sun, Y. D., Richoz, S., Krystyn, L., Zhang, Z. T., and Joachimski, M. M.: Perturbations in the carbon cycle during the Carnian Humid Episode: carbonate carbon isotope records from southwestern China and northern Oman, J. Geol. Soc., 176, 167–177, https://doi.org/10.1144/jgs2017-170, 2019.

Svensen, H., Planke, S., Chevallier, L., Malthe-Sørenssen, A., Corfu, F., and Jamtveit, B.: Hydrothermal venting of greenhouse gases triggered Early Jurassic global warming, Earth Planet. Sci. Lett., 256, 554–566, https://doi.org/10.1016/j.epsl.2007.02.013, 2007.

Them, T. R., Gill, B. C., Selby, D., Gröcke, D. R., Friedman, R. M., and Owens, J. D.: Evidence for rapid weathering response to climatic warming during the Toarcian Oceanic Anoxic Event, Sci. Rep., 7, 5003, https://doi.org/10.1038/s41598-017-05307-y, 2017.

Tomimatsu, Y., Nozaki, T., Sato, H., Takaya, Y., Kimura, J., Chang, Q., Naraoka, H., Rigo, M. and Onoue, T.: Marine osmium isotope record during the Carnian "Pluvial Episode" (Late Triassic) in the pelagic Panthalassa Ocean, Global Planet. Change, 197, 103387, https://doi.org/10.1016/j.gloplacha.2020.103387, 2021.

Tosca, N. J., Johnston, D. T., Mushegian, A., Rothman, D. H., Summons, R. E., and Knoll, A. H.: Clay mineralogy, organic carbon burial, and redox evolution in Proterozoic oceans, Geochim. Cosmochim. Ac., 74, 1579–1592, https://doi.org/10.1016/j.gca.2009.12.001, 2010.

Tremolada, F., van de Schootbrugge, B., and Erba, E.: Early Jurassic schizosphaerellid crisis in Cantabria, Spain: implications for calcification rates and phytoplankton evolution across the Toarcian Oceanic Anoxic Event, Paleoceanography, 20, PA2011, https://doi.org/10.1029/2004PA001120, 2005.

Trotter, J. A., Williams, I. S., Nicora, A., Mazza, M., and Rigo, M.: Long-term cycles of Triassic climate change: a new δ18O record from conodont apatite, Earth Planet. Sci. Lett., 415, 165–174, https://doi.org/10.1016/j.epsl.2015.01.038, 2015.

Ullmann, C. V., Boyle, R., Duarte, L. V., Hesselbo, S. P., Kasemann, S. A., Klein, T., Lenton, T. M., Piazza, V., and Aberhan, M.: Warm afterglow from the Toarcian Oceanic Anoxic Event drives the success of deep-adapted brachiopods, Sci. Rep., 10, 6549, https://doi.org/10.1038/s41598-020-63487-6, 2020.

Wang, X., Bachmann, G. H., Hagdorn, H., Sander, P. M., Cuny, G., Chen, X., Wang, C., Chen, L., Cheng, L., Meng, F., and Xu, G.: The Late Triassic black shales of the Guanling area, Guizhou Province, South-West China: a unique marine reptile and pelagic crinoid fossil Lagerstätte, Palaeontology, 51, 27–61, https://doi.org/10.1111/j.1475-4983.2007.00735.x, 2008.

Warrington, G. and Ivimey-Cook, H. C.: Triassic, Geol. Soc. Lond. Mem., 13, 97–106, https://doi.org/10.1144/GSL.MEM.1992.013.01.11, 1992.

Warrington, G.: The Permian, Triassic and Jurassic in Northern Ireland: a palynological study with special reference to the hydrocarbon prospectivity of the Larne–Lough Neagh Basin, Geological Survey of Northern Ireland Technical Report, GSNI/95/7, 1995.

Wilson, H. E. and Manning, P. I.: Geology of the Causeway Coast: Memoir for One-Inch Geological Sheet 7, Vol. 2, Geological Survey of Northern Ireland, H.M. Stationery Office, Belfast, 75–78, 1978.

Xu, G., Hannah, J. L., Stein, H. J., Mørk, A., Vigran, J. O., Bingen, B., Schutt, D. L., and Lundschien, B. A.: Cause of Upper Triassic climate crisis revealed by Re–Os geochemistry of Boreal black shales, Palaeogeogr. Palaeocl., 395, 222–232, https://doi.org/10.1016/j.palaeo.2013.12.027, 2014.

Xu, W., Ruhl, M., Jenkyns, H. C., Hesselbo, S. P., Riding, J. B., Selby, D., Naafs, B. D. A., Weijers, J. W. H., Pancost, R. D., Tegelaar, E. W., and Idiz, E. F.: Carbon sequestration in an expanded lake system during the Toarcian Oceanic Anoxic Event, Nat. Geosci., 10, 129–134, https://doi.org/10.1038/ngeo2871, 2017.

Xu, W., Ruhl, M., Jenkyns, H. C., Leng, M. J., Huggett, J. M., Minisini, D., Ullmann, C. V., Riding, J. B., Weijers, J. W. H., Storm, M. S., Percival, L. M. E., Tosca, N. J., Idiz, E. F., Tegelaar, E. W., and Hesselbo, S. P.: Evolution of the Toarcian (Early Jurassic) carbon-cycle and global climatic controls on local sedimentary processes, Cardigan Bay Basin, UK, Earth Planet. Sci. Lett., 484, 396–411, https://doi.org/10.1016/j.epsl.2017.12.037, 2018.

Yang, J., Cawood, P. A., Du, Y., Li, W., and Yan, J.: Reconstructing Early Permian tropical climates from chemical weathering indices, Geol. Soc. Am. Bull., 128, 739–751, https://doi.org/10.1130/B31371.1, 2016.

Yuan, G., Cao, Y., Gluyas, J., Li, X., Xi, K., Wang, Y., Jia, Z., Sun, P., and Oxtoby, N. H.: Feldspar dissolution, authigenic clays, and quartz cements in open and closed sandstone geochemical systems during diagenesis: typical examples from two sags in Bohai Bay Basin, East China, AAPG Bull., 99, 2121–2154, https://doi.org/10.1306/07101514004, 2015.

Zhang, P., Yang, M., Lu, J., Jiang, Z., Zhou, K., Xu, X., Wang, Y., Wu, S., Chen, H., Zhu, X., Guo, W., Ye, M., Shao, L., and Hilton, J.: Floral response to the Late Triassic Carnian Pluvial Episode, Front. Ecol. Evol., 11, 1199121, https://doi.org/10.3389/fevo.2023.1199121, 2023.

Zhang, P., Yang, M., Lu, J., Jiang, Z., Vervoort, P., Zhou, K., Xu, X., Chen, H., Wang, Y., He, Z., Bian, X., Shao, L., and Hilton, J.: Four volcanically driven climatic perturbations led to enhanced continental weathering during the Late Triassic Carnian Pluvial Episode, Earth Planet. Sci. Lett., 626, 118517, https://doi.org/10.1016/j.epsl.2023.118517, 2024a.

Zhang, Q., Fu, X., Wang, J., Mansour, A., Wei, H., Zhang, T., and Wang, M.: Orbitally paced climate change during the Carnian Pluvial Episode, Earth Planet. Sci. Lett., 626, 118546, https://doi.org/10.1016/j.epsl.2023.118546, 2024b.

https://doi.org/10.5194/egusphere-2026-2964
Preprint. Discussion started: 21 July 2026

Zhang, Y., Li, M., Ogg, J. G., Montgomery, P., Huang, C., Chen, Z. Q., Shi, Z., Enos, P., and Lehrmann, D. J.: Cycle-calibrated magnetostratigraphy of middle Carnian from South China: implications for Late Triassic time scale and termination of the Yangtze Platform, Palaeogeogr. Palaeocl., 436, 135–166, https://doi.org/10.1016/j.palaeo.2015.05.033, 2015.

Zhao, H., Grasby, S. E., Wang, X., Zhang, L., Liu, Y., Chen, Z.Q., Hu, Z., and Huang, Y.: Mercury enrichments during the Carnian Pluvial Event (Late Triassic) in South China, Geol. Soc. Am. Bull., 134, 2709–2720, https://doi.org/10.1130/B36205.1, 2022.

Zhao, X., Xue, N., Yang, H., Zheng, D., Peng, J., Frieling, J., De Vleeschouwer, D., Fu, X., Jia, W., Fang, Y., Li, S., Wang, M., Zhao, X., Wang, Q., Zhang, H., Sha, J., Jenkyns, H. C., Claeys, P., and Wang, B.: Climate–carbon-cycle interactions and spatial heterogeneity of the late Triassic Carnian Pluvial Episode, Nat. Commun., 16, 5404, https://doi.org/10.1038/s41467-025-61262-7, 2025.